J. Fluid Mech. (2012), *vol.* 710, *pp.* 195–233.
doi:10.1017/jfm.2012.359

Flow around six in-line square cylinders

C. M. Sewatkar[1], Rahul Patel[2], Atul Sharma[2] and Amit Agrawal[2,1]†

[1] Department of Mechanical Engineering, College of Engineering, Pune 411005, India

[2] Department of Mechanical Engineering, Indian Institute of Technology Bombay, Powai, Mumbai 400076, India

(Received 21 September 2011; revised 8 July 2012; accepted 10 July 2012; first published online 3 September 2012)

The flow around six in-line square cylinders has been studied numerically and experimentally for $0.5 \leqslant s/d \leqslant 10.0$ and $80 \leqslant Re \leqslant 320$, where s is the surface-to-surface distance between two cylinders, d is the size of the cylinder and Re is the Reynolds number. The effect of spacing on the flow regimes is initially studied numerically at $Re = 100$ for which a *synchronous* flow regime is observed for $0.5 \leqslant s/d \leqslant 1.1$, while *quasi-periodic-I*, *quasi-periodic-II* and *chaotic* regimes occur between $1.2 \leqslant s/d \leqslant 1.3$, $1.4 \leqslant s/d \leqslant 5.0$ and $6.0 \leqslant s/d \leqslant 10.0$, respectively. These regimes have been confirmed via particle-image-velocimetry-based experiments. A flow regime map is proposed as a function of spacing and Reynolds number. The flow is predominantly quasi-periodic-II or chaotic at higher Reynolds numbers. The quasi-periodic and chaotic nature of the flow is due to the wake interference effect of the upstream cylinders which becomes more severe at higher Reynolds numbers. The appearance of flow regimes is opposite to that for a row of cylinders. The Strouhal number for vortex shedding is the same for all the cylinders, especially for synchronous and quasi-periodic-I flow regimes. The mean drag (C_{Dmean}) experienced by the cylinders is less than that for an isolated cylinder, irrespective of the spacing. The first cylinder is relatively insensitive to the presence of downstream cylinders and the C_{Dmean} is almost constant at 1.2. The C_{Dmean} for the second and third cylinders may be negative, with the value of C_{Dmean} increasing monotonically with spacing. The changes in root mean square lift coefficient are consistent with changes in C_{Dmean}. Interestingly, the instantaneous lift force can be larger than the instantaneous drag force on the cylinders. These results should help improve understanding of flow around multiple bluff bodies.

Key words: flow-structure interactions, interacting wakes, low-Reynolds-number flows

1. Introduction

Study of fluid flow and vorticity dynamics across bluff bodies serves as a model for understanding flow around more complex structures. The flow across six identical square cylinders placed one behind the other (in-line or tandem configuration) has been studied in this work. Part of the motivation for exploring flow across a large number of in-line cylinders comes from observations for two cylinders where the drag on the downstream cylinder becomes negative; another interesting phenomenon is lock-on in vortex shedding from two in-line cylinders. Whether these observations

† Email address for correspondence: amit.agrawal@iitb.ac.in

can be extended to a system of more than two cylinders in the flow is not clear and needs to be explored. We have arbitrarily chosen six cylinders, which is representative of a sufficiently large size. It is however expected that the flow around the last few cylinders will become independent of the cylinder number when a large number of cylinders are actually present.

The present study is undertaken with a view to: (i) documenting the flow patterns that the flow can exhibit, (ii) comparing the results for multiple cylinders with those for two tandem cylinders, (iii) comparing the results for square cylinders with those for circular cylinders, and (iv) throwing light on flow phenomena when cylinders are arranged in tandem versus a side-by-side configuration. The study is also relevant to evaluation of the aerodynamic performance of trains and motor vehicles, and structural design of buildings, bridges, heat exchangers, etc. The relevant non-dimensional governing parameters for such flows are spacing (s/d) and Reynolds number ($Re = U_0 d/\nu$), where s is the surface-to-surface distance between cylinders, d is size of the cylinder, U_0 is the uniform inlet velocity, and ν is the kinematic viscosity of the fluid.

Flow past two in-line square cylinders is one of the simpler cases of flow across an array of cylinders and has been studied both experimentally and numerically. Among the experimental works, Sakemoto, Haniu & Obata (1987) investigated forces acting on two in-line square cylinders in a uniform flow at $Re = 2.67 \times 10^4$ and 5.52×10^4; they observed different flow patterns below and above a critical spacing of $s/d = 3$. Two different values of the mean drag coefficient (C_D) and Strouhal number (St) have been reported due to the existence of the different flow patterns (Sakemoto *et al.* 1987; Luo & Teng 1990; Liu & Chen 2002). For two square cylinders, Liu & Chen (2002) further reported the occurrence of hysteresis accompanied by two discontinuous jumps for all the Reynolds numbers studied ($Re = 2.0 \times 10^3$–1.6×10^4), as the spacing is either progressively increased or decreased. The hysteresis was again associated with the existence of two different flow patterns. In the first flow pattern at small spacings (Mode I), roll-up of the shear layer separated from the upstream cylinder is suppressed. In the second flow pattern that appears at larger spacings (Mode II), the shear layer separated from the upstream cylinder periodically rolls up to form vortices, and the rolled-up vortices interact with the downstream cylinder. The discontinuous jumps are attributed to a sudden change in the flow pattern between Modes I and II. Yen, San & Chuang (2008) studied the effect of Reynolds number, spacing and rotation angle of the downstream cylinder using particle image velocimetry (PIV) and topological analysis for two in-line square cylinders. Based on the Reynolds number, the flow was categorized into a vortex street of single mode, reattached mode, or binary mode. The Strouhal number decreases as the Reynolds number increases (for $Re < 405$), and subsequently increases asymptotically. Kim *et al.* (2008) divided the flow around two in-line square cylinders into two different flow patterns separated by the critical spacing of $s/d = 2.5$, for $Re = 5300$ and 16 000. The Mode I pattern had large recirculation regions between the two cylinders caused by the separated shear layer of the upstream cylinder that reattached on the lateral surface of the downstream cylinder. The Mode II pattern had separated shear layers at both the upstream and downstream cylinders. In terms of the vortex shedding frequency Kim *et al.* (2008) noticed behaviour similar to that reported by Yen *et al.* (2008). Sohankar & Etminan (2009) numerically studied the flow around two in-line square cylinders for $1 \leqslant Re \leqslant 200$. Their result suggests that the onset of vortex shedding occurs in the range of $Re = 35$–40 for $s/d = 5$. They found that the flow separates from the cylinder rear corners in the range of $1 < Re \leqslant 2$ for the upstream

cylinder and $2 < Re \leqslant 5$ for the downstream cylinder. Further, the location of the flow separation changes from the rear to the front corners of the upstream cylinder in the range of $100 < Re \leqslant 125$. The level of the force fluctuations on the downstream cylinder is larger than the corresponding values for the upstream one, due to the flow interaction of the upstream cylinder with the downstream one. Lankadasu & Vengadesan (2007) investigated interference effect of two equal-sized square cylinders in tandem arrangement, immersed in a planar shear flow. They found that the root mean square (r.m.s.) values for both lift and drag increase and then decrease for upstream cylinder with increasing spacing; whereas these values increase continuously for the downstream cylinder.

Many researchers have studied flow past two in-line *circular* cylinders. The typical regimes reported are single bluff body, shear layer reattachment, and synchronization of vortex shedding from the cylinders. Wang *et al.* (2010) revisited these regimes in their experimental study to investigate the dependence of Strouhal number on spacing and to explore the flow characteristics relevant to critical spacing and hysteretic mode of transitions at critical spacing. Mittal, Kumar & Raghuvanshi (1997) reported that when the flow becomes unsteady, the downstream cylinder, which lies in the wake of the upstream cylinder, experiences relatively large unsteady forces that may lead to wake-induced flutter. Carmo, Meneghini & Sherwin (2010*a*) proposed that if the separation is less than the drag inversion spacing, the downstream cylinder has a stabilizing effect on the flow. For such cases, the three-dimensional structures appeared later in terms of Reynolds number than for the flow around an isolated cylinder. On the other hand, if the separation is greater than the drag inversion spacing, the initial stages of the transition in the wake occurred in a similar way to that of an isolated cylinder. Their comprehensive study shows the different ways in which the stages of the transition scenario respond to flow interference. A comprehensive and recent review of literature on two cylinders is available in Sumner (2010).

There are relatively few studies with multiple (>2) in-line cylinders in the flow. Harichandan & Roy (2010) obtained steady wake patterns at $Re = 100$ and sparse von Kármán vortex street at $Re = 200$, with three in-line circular cylinders. The unsteady forces experienced by the cylinders are also documented in their numerical study; the forces become more severe at small spacings ($s/d = 1.0$). When the longitudinal gap is increased ($s/d = 4.0$), there was no flow separation or reattachment of the shear layer from the upstream cylinder to the immediate downstream cylinder; instead, von Kármán vortex streets were observed between the cylinders. However, the vortex shedding from the downstream cylinder was highly disturbed by the impingement of the upstream vortex streets emerging from the uppermost and middle cylinders. A gap vortex shedding mechanism was proposed by Hetz, Dhaubhadel & Telionis (1991), who experimentally studied the flow around five in-line circular cylinders (known as a pentad). For $s/d = 0.1$–0.8 with $Re = 1 \times 10^4$–5×10^4, it was conjectured that such a gap vortex shedding mechanism is present in the flow across a bank of cylinders and could be excited if driven by structural vibrations. Liang, Papadakis & Luo (2009) studied the flow around six in-line circular cylinders for $1.1 \leqslant s/d \leqslant 3.0$ at $Re = 100$. They proposed that an increase in the spacing makes the flow more asymmetric and induces vortex shedding starting from the last cylinder and proceeding upstream. Further, the force statistics are maximized in the spacing region of $s/d = 2.0$–2.6 and then drops drastically at $s/d = 3$ for the last three cylinders. Some of these observations are tested further as part of the present work.

Thus, it is noticed from the literature survey that the flow behaviour for a large number of in-line cylinders is not well studied. Our purpose here is to extend

the works of Hetz *et al.* (1991) and Liang *et al.* (2009) by performing a detailed numerical and a limited experimental study of flow around large in-line square cylinders, which is a problem of significant fundamental interest besides being of engineering importance. The number of cylinders is deemed to be large enough to model a large number of bodies and also mimics the configuration studied earlier by Hetz *et al.* (1991) and Liang *et al.* (2009). The flow regimes as a function of spacing and Reynolds number are first identified from the numerical data and then confirmed through experiments. The other important objectives of this work are to document the variation of engineering parameters (Strouhal number, drag coefficient and lift coefficient) as a function of spacing, along with uncovering the underlying flow physics.

2. Physical description of the problem

The physical problem considered here is flow across six square cylinders arranged in-line as shown in figure 1(*a*). All cylinders are of identical size with the same distance between two consecutive cylinders. The leading cylinder with side d, which is also the characteristic length scale, is exposed to a constant and uniform velocity, U_0. The streamwise length of the computational domain is given by $lx = L_u + L_d + d + (d + s)(n - 1)$, where L_u is the upstream length from the inlet of the domain to the front surface of the first cylinder (denoted by C_1 in figure 1*a*), L_d is the downstream length from the rear of the last cylinder (denoted by C_6 in figure 1*a*), and n is the number of cylinders. The free-slip boundary on the lateral side extends up to $10d$ on either side of the cylinders. Domain-independent results are obtained for $L_u = 7d$, $L_d = 32d$ and $l_y = 21d$. The streamwise direction is denoted as x and the cross-stream direction as y, with the origin of the coordinate system fixed at the middle of the front surface of the first cylinder (see figure 1*a*).

2.1. *Numerical details*

The two-dimensional lattice Boltzmann method (LBM) is used in this study. The assumption of two-dimensionality can be justified due to the small value of Reynolds number employed here ($Re \leqslant 160$ for the simulations). The basic principle of LBM involves movement of particles on a lattice. The computational lattice unit is square, with one at rest and eight moving particles. The particles collide at each time step, and change in their velocity occurs; however, the net mass and momentum are conserved during collisions. Therefore, propagation of particles and their collision form the two basic steps of this method. The method has second-order spatial accuracy. Ease of introducing the obstacle in the flow is the most important advantage of this method, and hence LBM is ideally suited to the present study.

The discrete kinetic equation used in LBM for the particle distribution is

$$f_i(x + e_i\Delta t, t + \Delta t) = f_i(x, t) - \frac{\Delta t}{\tau}(f_i(x, t) - f_i^{eq}(x, t)), \quad i = 0, 1, \ldots, 8, \tag{2.1}$$

where f_i is the instantaneous particle density at a link, f_i^{eq} is the corresponding equilibrium density, e_i is the particle velocity in the i-direction, τ is the relaxation time, Δt is the time step (unity in the present case), and x, y, respectively, represent coordinates along the streamwise and transverse directions. The equilibrium function is calculated as

$$f_i^{eq} = \rho w_i(1 + 3(e_i \cdot u) + \tfrac{9}{2}(e_i \cdot u)^2 - \tfrac{3}{2}u^2), \tag{2.2}$$

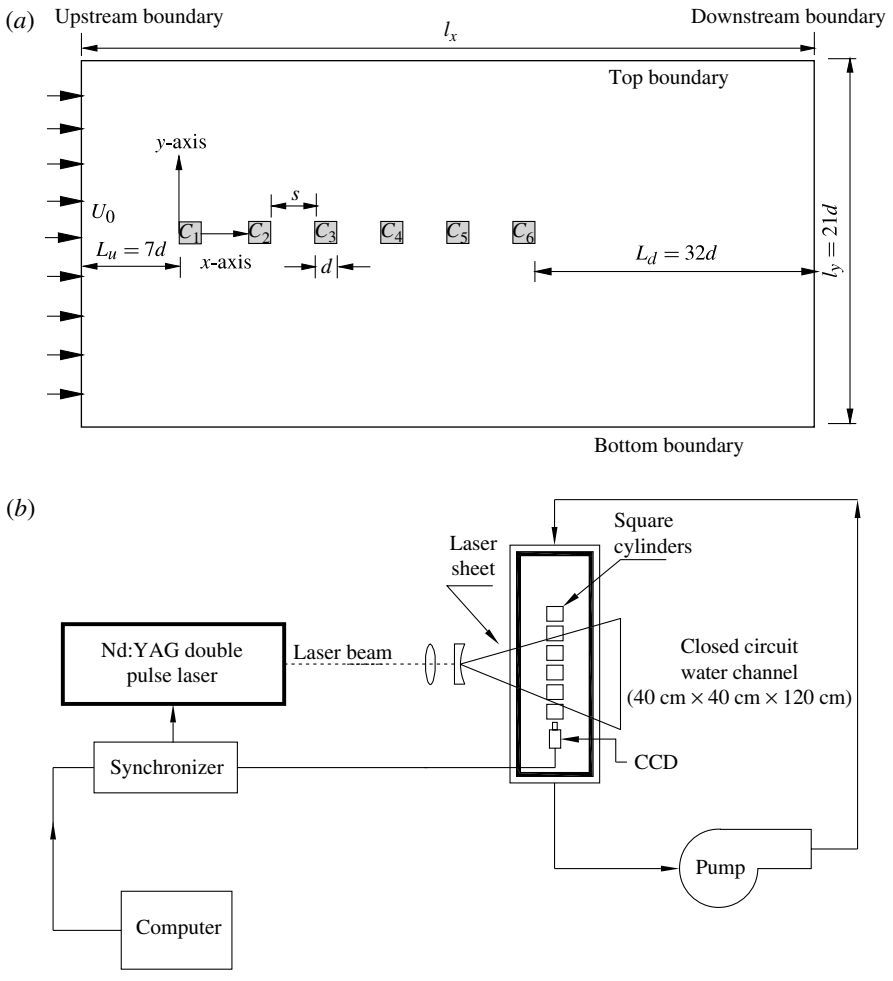

FIGURE 1. (*a*) The computational domain. Note that the origin of the coordinate axis is located at the centre of the front surface of the first cylinder. The cylinders have been marked as C_1–C_6 starting from the left. (*b*) Schematic of the experimental setup.

where ρ $(=\Sigma_i f_i)$ is the fluid density, u $(\rho u = \Sigma_i f_i e_i)$ is the local fluid velocity, and w_i are the corresponding weights (4/9 for the rest particle, 1/9 for each of the four axial particles, 1/36 for each of the diagonal particles). The relaxation time is related to the kinematic viscosity (ν) of the fluid via the following equation:

$$\nu = \frac{2\tau - 1}{6}. \tag{2.3}$$

Equation (2.1) is solved in two steps, namely collision and propagation. Mathematically these steps can be expressed as (collision)

$$f_i^{new}(x, t) = f_i(x, t) - \frac{\Delta t}{\tau}(f_i(x, t) - f_i^{eq}(x, t)), \tag{2.4}$$

	Re	s/d	Method
Numerical	100	0, 0.5;	LBM
	40, 60, 80, 120, 140, 150 and 160	1.0–1.5 in step of 0.1; 2.0–4.0 in step of 0.5; 5.0–10.0 in step of 1 0.5–4 in step of 0.5; 5.0 and 6.0	
Experimental	100	0.5, 1.0, 2.0 and 4.0	PIV and flow visualization
	150 and 320	0.5, 1.0, 2.0 and 4.0	PIV

TABLE 1. Governing parameters considered and the methods used in the numerical and experimental study.

where f_i^{new} is an intermediate function, and (propagation)

$$f_i(x + e_i\Delta t, t + \Delta t) = f_i^{new}(x, t). \tag{2.5}$$

It is reported in the literature (Frisch, Hasslacher & Pomeau 1986; Chen & Doolen 1998; Succi 2001; Djenidi 2006) that solving the particle distribution equation (equation (2.1)) is equivalent to solving the Navier–Stokes equation. The theoretical basis of LBM can also be found in these references. The code employed for the present study is essentially the same as used in our earlier works (Agrawal, Djenidi & Antonia 2006; Kumar, Sharma & Agrawal 2008; Sewatkar, Sharma & Agrawal 2009, 2010, 2011, 2012).

A uniform and square grid is employed in the simulations. The cylinder is appropriately resolved to obtain grid-independent results (a minimum of 24 points on one side of the cylinder). A uniform velocity (U_0) with negligible compressibility effect is prescribed at the inlet boundary. Free-slip boundary conditions have been applied on the lateral edges of the computational domain. A convective boundary condition is used at the outlet to ensure unconstrained movement of fluid away from the computational domain (Sewatkar *et al.* 2011). The bounceback condition is used at the walls of the cylinders in order to simulate the no-slip condition; see Agrawal & Agrawal (2006) for implementation details of the bounceback condition. Simulations start with the flow initially at rest. Each simulation is run for at least 8 secondary cycles. A secondary cycle encompasses 4–7 primary cycles; the time period for one vortex shedding is about 6000 time steps. The initial transient variation of engineering parameters such as drag coefficient are not included in the computed statistics. The code has been validated for both single and multiple cylinders as presented earlier (Agrawal *et al.* 2006; Kumar *et al.* 2008; Sewatkar *et al.* 2009, 2011). The range of the governing parameters considered in the detailed numerical study is given in table 1.

2.2. *Experimental details*

The experiments are conducted using PIV in a closed-circuit water channel made of a 1.5 cm thick acrylic sheet of outer dimensions 120 cm × 40 cm × 40 cm; see figure 1(*b*) for a schematic of the experimental setup. Water is pumped into the channel using a 6 l s^{-1} capacity pump which produced a flow velocity of 0.8–4 cm s^{-1}. The entire

water channel is seeded with spherical hollow-glass particles (from Potter Industries Inc., Australia; mean particle size of 8–11 μm, density around 1.1 g cm^{-3}, made of fused borosilicate glass). A double pulsed light sheet is produced by dual Nd:YAG lasers (Beamtech, China; energy 200 mJ $pulse^{-1}$, repetition rate 15 Hz, wavelength 532 nm). An inter-line CCD camera is used to capture the images (PCO, Germany; image size 1392 × 1024 pixels, frame rate 10 Hz). Square acrylic cylinders of size 10 mm × 10 mm are used in the experiments. The timing of laser firing and CCD capture is controlled by a synchronizer (from Beamtech). The time separation between the two laser pulses is typically 100 ms.

The PIV frames are captured at 1 Hz. The data set for a given case comprises 138 pairs of statistically independent images. The images obtained from the camera are processed using a commercial code to obtain velocity vectors and vorticity contours. Standard multi-pass cross-correlation analysis is used to convert the raw data into a velocity field. The spacing between two vectors is about 2 mm. The typical error in velocity measurement is estimated as 2 %.

The experimental setup was validated by comparing results for flow over a single square cylinder with the available literature. Subsequently, experiments were conducted with six in-line square cylinders for the range of parameters given in table 1. A limited flow visualization study was also undertaken in the same water channel. Potassium permanganate was used as the dye for this study, while a digital camera was used for recording the images. Flow visualization is restricted to $Re = 100$ with $s/d = 0.5$, 1.0, 2.0 and 4.0.

2.3. *Sensitivity to number of cylinders*

As mentioned above, our aim is to simulate the flow around a large number of in-line cylinders. In this section, we examine the minimum number of cylinders required to simulate such a flow. Preliminary simulations are carried out by varying the number of cylinders from four to ten, at $s/d = 1.2$ and $Re = 100$. As explained later in § 3.2, the flow exhibits quasi-periodic-I behaviour for six cylinders (the $n = 6$ case) at these parameter values. This regime is sufficiently interesting and complicated, and is therefore selected to explore the effect of the number of cylinders on flow behaviour.

The r.m.s. of the lift coefficient versus cylinder number for the various cases is shown in figure 2(*a*). Notice that $C_{L,rms}$ for the $n = 4$ case is substantially smaller than the other cases. $C_{L,rms}$ for the $n = 5$ case approaches the value obtained with the $n > 5$ cases, with a marked deviation in the value for the last cylinder. $C_{L,rms}$ for the $n = 6$ case approaches even more closely the value obtained with $n > 6$ cases; a marked deviation in the value for the last cylinder is again observed (this latter observation applies to the $n > 6$ cases too). The mean of the drag coefficient versus cylinder number for the various cases is shown in figure 2(*b*). Notice that $C_{D,mean}$ for $n = 6$ case compares well with $4 \leqslant n \leqslant 8$ cases (which are lower than $n = 9, 10$ cases) for all the cylinders. The above results bring out the complicated behaviour of the flow with number of cylinders.

The number of cylinders is arbitrarily chosen and is fixed at six for further computations. This number appears sufficient to simulate a large number of in-line cylinders.

3. Numerical study of flow regimes

The purpose of this section is to examine the various flow regimes with six in-line cylinders. The various flow regimes reported for multiple cylinders are synchronous,

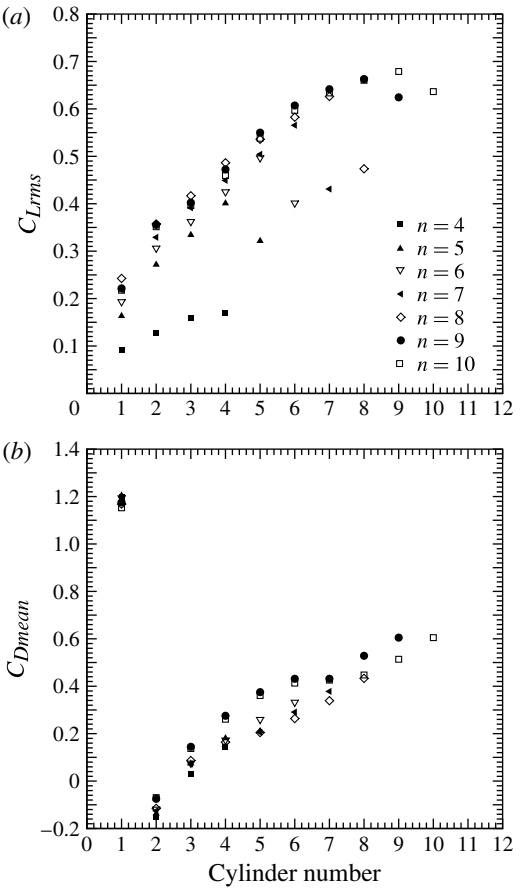

FIGURE 2. Variation of (*a*) r.m.s. lift coefficient, and (*b*) mean drag coefficient as a function of cylinder number for different numbers of cylinders actually present in the domain.

quasi-periodic-I, quasi-periodic-II and chaotic. Note that these regimes were reported for a row of square cylinders, using a numerical method (Kumar *et al.* 2008; Sewatkar *et al.* 2009). Here, we numerically verify the existence of these flow regimes for in-line cylinders and document their occurrence with respect to cylinder spacing. The flow regimes are confirmed through experiments in § 4. The effect of spacing on flow pattern, wake interaction, lift and drag coefficients, and vortex shedding was initially studied at $Re = 100$. This is an interesting case, as the Reynolds number is sufficiently large to capture the essential flow dynamics. Subsequently, in § 5, the effects of Reynolds number are discussed, with the purpose of verifying the findings at other Reynolds number values.

3.1. *Synchronous flow* ($s/d \leqslant 1.1$)

The instantaneous vorticity contours and streamlines for $s/d = 0.5$ and 1.0 are presented in figure 3. It is noticed that a single wake is formed behind the cylinders at these spacings, as if the flow is occurring over a single cylinder. Although formation of shear layer begins at the first cylinder itself, the vortex shedding occurs essentially behind the last cylinder. Notice that the waviness of the shear layer increases with

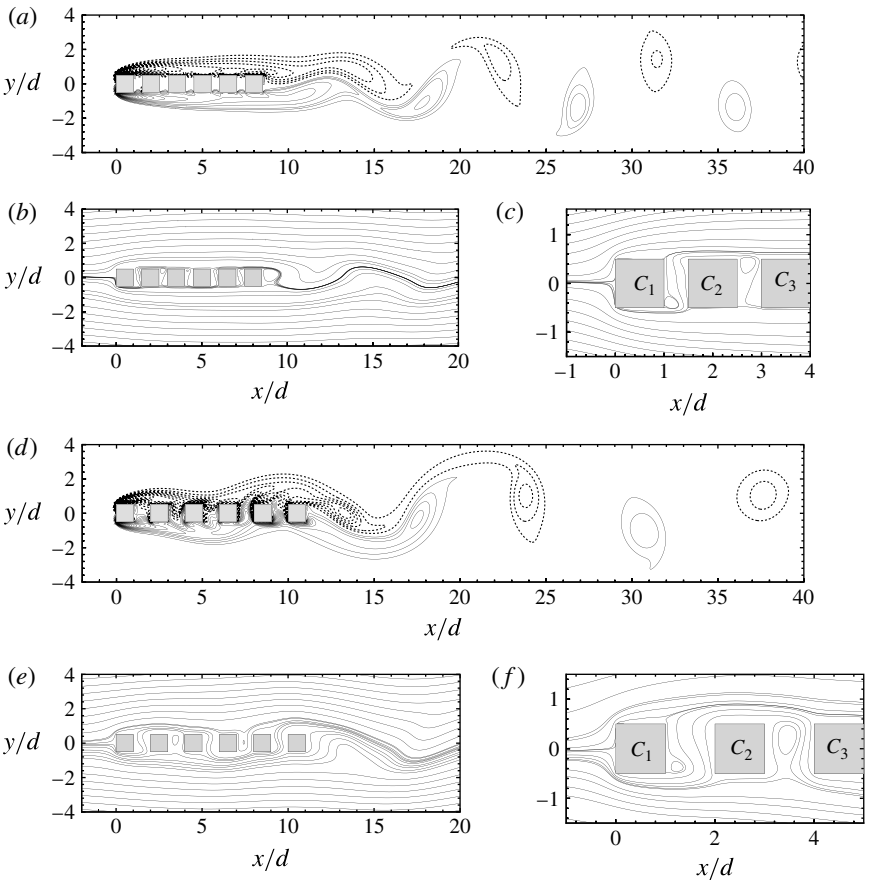

FIGURE 3. (*a,d*) Instantaneous vorticity contours, (*b,e*) streamlines, and (*c,f*) enlarged view of streamlines for (*a–c*) $s/d = 0.5$ and (*d–f*) $s/d = 1.0$ at $Re = 100$. The dashed lines in (*a,d*) indicate negative vorticity.

spacing (compare figure 3*a* with figure 3*d*). The streamline patterns in figures 3(*b*) and 3(*e*) indicate some crossing over of the fluid from top to bottom of the cylinders (or vice versa); this crossing over of fluid changes with spacing and leads to the formation of different flow regimes. The vortex shedding occurs essentially behind the last cylinder. The streamlines in figure 3(*c,f*) further indicate that vortices are formed in the gap near the top/bottom of the cylinders. This is in contrast to the circular cylinder results of Liang *et al.* (2009), where a pair of standing vortices is noticed in the gap regions at comparable values of spacing and Reynolds number ($s/d = 1.1$ and 1.3, $Re = 100$).

At $s/d = 0.5$, the time signals of the lift coefficient (C_L) and drag coefficient (C_D) for the six cylinders are shown in figures 4 and 5. The lift signal is almost sinusoidal in nature for all the cylinders (except cylinder 4) indicating the presence of a single frequency corresponding to the vortex shedding frequency. It is however important to reiterate that the vortex shedding takes place behind the last cylinder only (figure 3*a*), which leads to C_{L6} having the largest amplitude. The variation in lift for the first two cylinders is due to alternate formation of vortices in the gap region. These

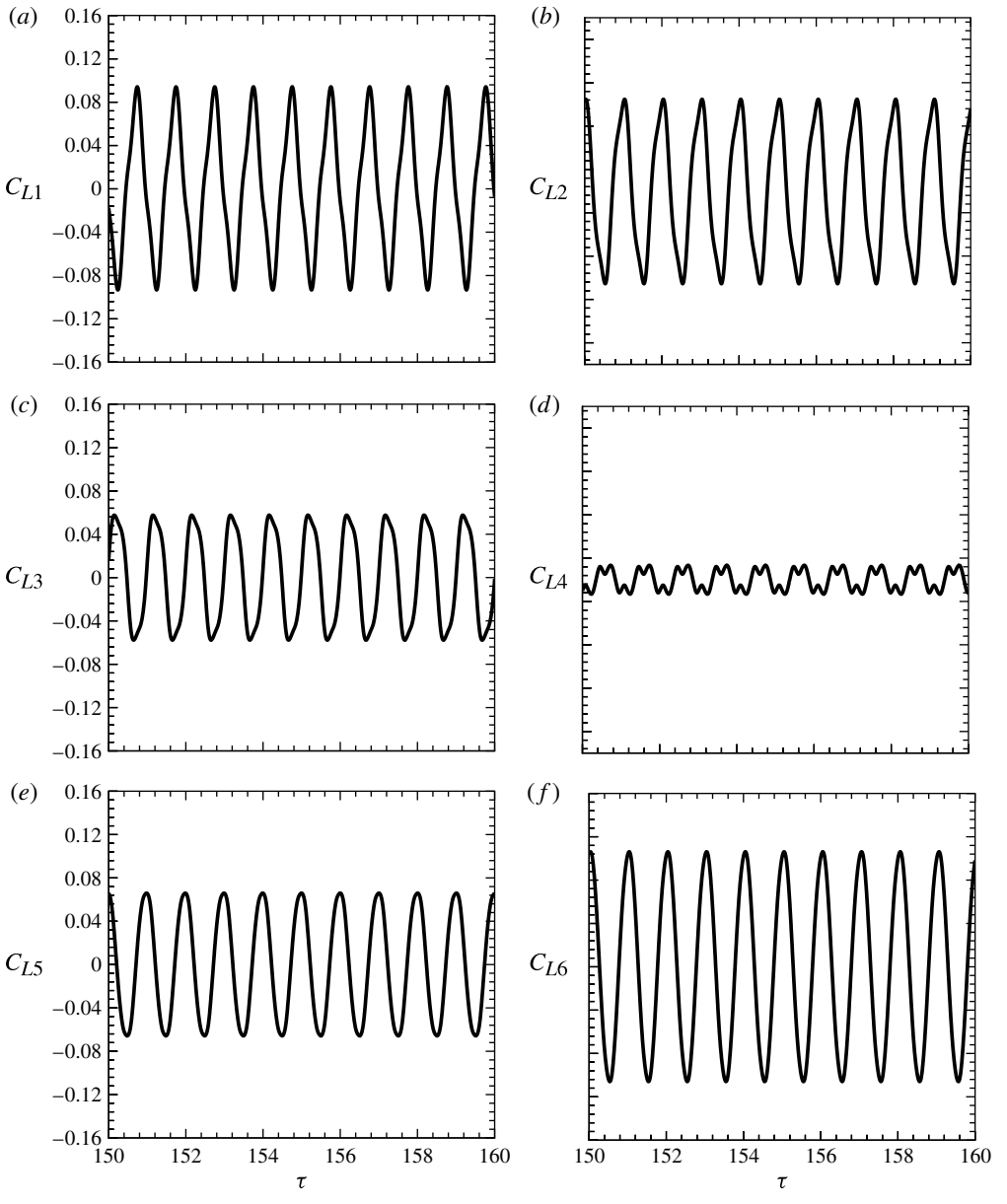

FIGURE 4. Time series of lift coefficient experienced by the cylinders at $s/d = 0.5$ and $Re = 100$.

vortices are however weak and small in size, and diffuse away quickly. The larger value of lift coefficient for cylinders 1, 2 and 6 (see figure 4*a,b,f* respectively) as compared to cylinder 4 (figure 4*d*) is due to the formation of vortices behind these cylinders. The pressure varies for these cylinders owing to change in the position of vortex behind these cylinders. The vortex location changes as the small vortices are diffused away. This explains the trend of maximum lift coefficient experienced by the cylinders, as plotted in figure 4. Figure 5 reveals that the signal for the drag

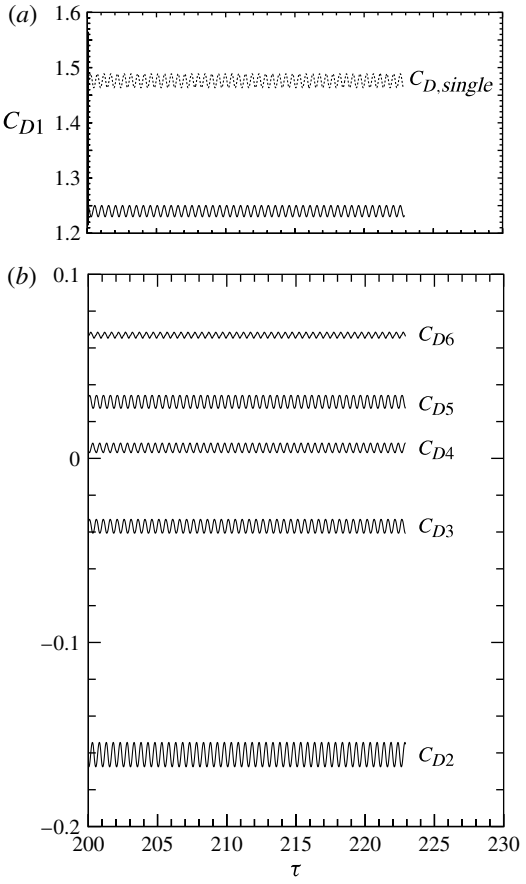

FIGURE 5. Time series of drag coefficient experienced by (*a*) cylinder 1 and (*b*) cylinders 2–6, at $s/d = 0.5$ and $Re = 100$. The dashed line in (*a*) represents the time series of drag coefficient on a single square cylinder at the same Reynolds number.

coefficient is also sinusoidal for all the cylinders. Further, the signals from consecutive cylinders are almost in anti-phase with respect to each other. This is due to the fact that vortices are formed in the gaps alternately from the top and bottom of the rear surface of consecutive cylinders. Notice that the upstream side of the first cylinder is subjected to the highest pressure in the domain while the downstream side of the sixth (last) cylinder is subjected to lowest pressure (figure 34*a*, explained later). The pressure gradient experienced in either direction by the other cylinders is however comparatively low, because all the cylinders are enveloped inside the same wake.

Similar signals of lift and drag coefficients are also noticed for $s/d = 1.0$ and 1.1. The Strouhal numbers based on the lift signal are calculated for all the cylinders using power spectral analysis. The power spectrum for $s/d = 0.5$ shown in figure 6 indicates a single frequency, which confirms the sinusoidal nature of the lift signal. The value of Strouhal number in this case is the same for all the cylinders, as shown in figure 6 for selected cylinders (cylinders 2–4). Thus, at small spacings ($s/d \leqslant 1.1$), using the terminology of Kumar *et al.* (2008), the flow can be termed as *synchronous* in nature.

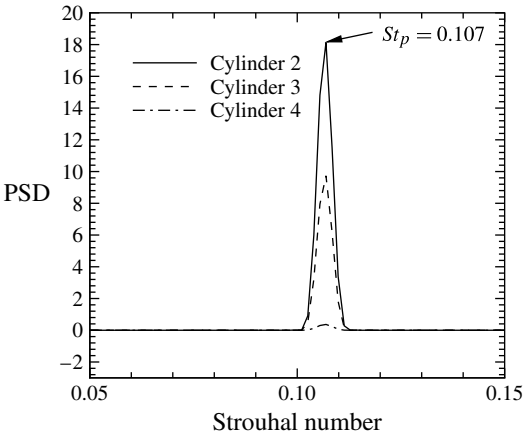

FIGURE 6. Power spectra at $s/d = 0.5$ and $Re = 100$ for selected cylinders.

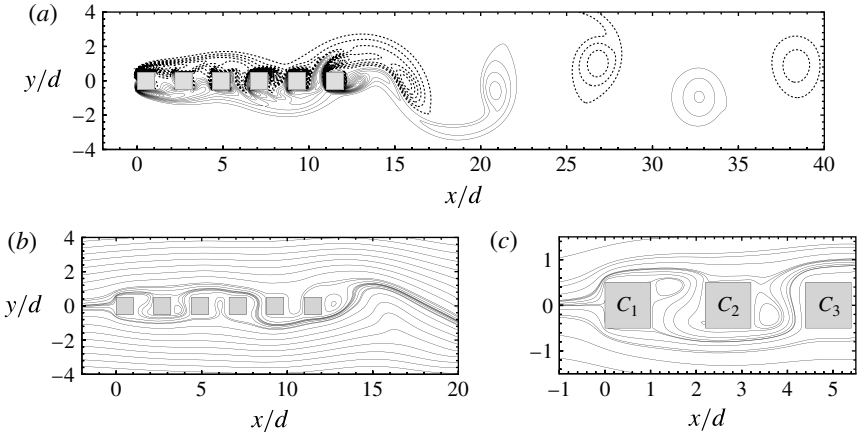

FIGURE 7. (*a*) Instantaneous vorticity contours, (*b*) streamlines, and (*c*) enlarged view of streamlines for $s/d = 1.2$ and $Re = 100$. The dashed lines in (*a*) indicate negative vorticity.

3.2. *Quasi-periodic-I flow* ($1.2 \leqslant s/d \leqslant 1.3$)

As discussed above, the flow is synchronous for $s/d \leqslant 1.1$, and as explained later in § 3.3, the flow becomes quasi-periodic-II for $s/d \geqslant 1.4$. Between $s/d = 1.0$ and 1.5, simulations in a finer step of 0.1 were undertaken in order to resolve the flow transition from synchronous to quasi-periodic-II. The instantaneous vorticity contours and streamlines for $s/d = 1.2$ are shown in figure 7. It is noticed that the vortex shedding occurs essentially behind the last cylinder. The streamline pattern shows that the vortices are formed in the gap from near the top and bottom of the vertical surfaces of the cylinders, alternately with time.

The signals of lift and drag coefficients for $s/d = 1.2$ are shown in figures 8 and 9, respectively. These signals do not show the sinusoidal variation of C_L or C_D signals of an isolated cylinder, or of figures 4 and 5; rather, these signals are modulated. These modulations indicate the presence of a secondary frequency in the

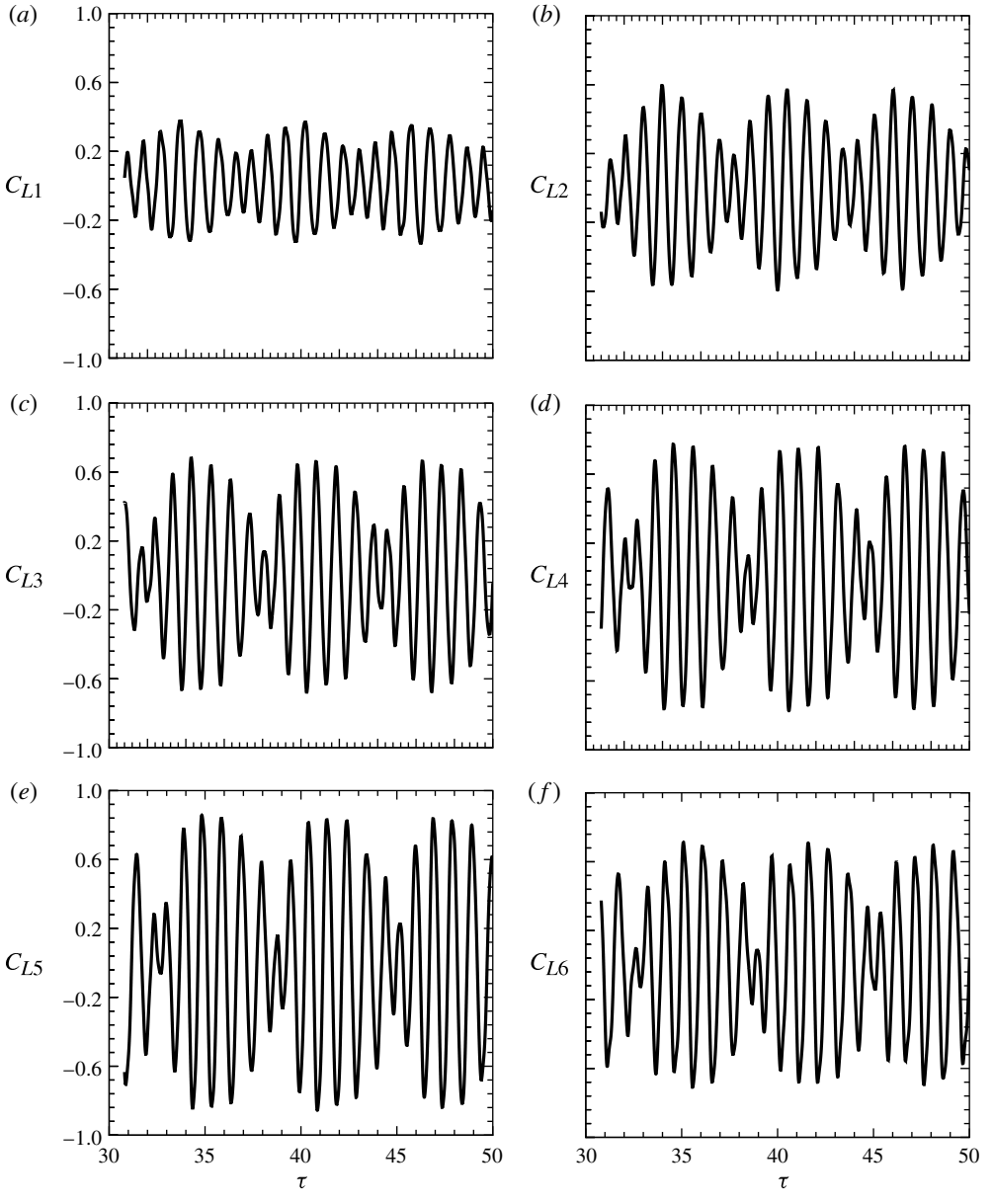

FIGURE 8. Time series of lift coefficient experienced by the cylinders at $s/d = 1.2$ and $Re = 100$.

signal which spans over seven vortex shedding (primary) cycles. It is noticed that the cycle-to-cycle variation in the time period of the primary (vortex shedding) frequency is less than 5 %, whereas it is constant for the secondary frequency in this regime. This has been rigorously verified for a large number of secondary cycles. The power spectrum of the lift coefficient (figure 10) indeed shows the presence of two peaks, each corresponding to the primary (vortex shedding) and secondary frequencies. The peak at $St_p = 0.079$ corresponds to the primary (or vortex shedding frequency) while a

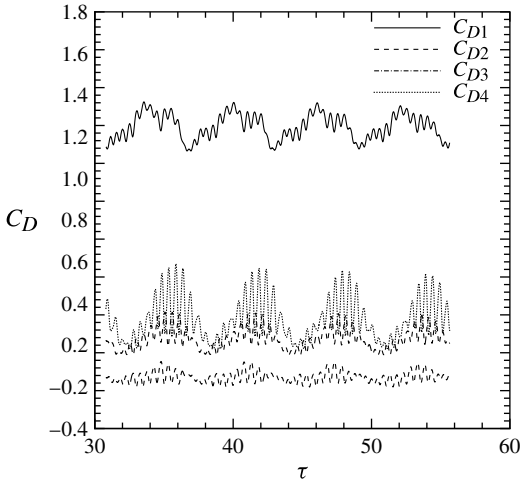

FIGURE 9. Time series of drag coefficient experienced by selected cylinders at $s/d = 1.2$ and $Re = 100$.

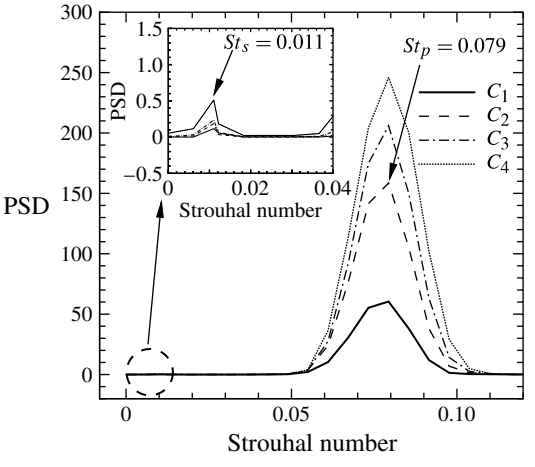

FIGURE 10. Power spectra at $s/d = 1.2$ and $Re = 100$ for selected cylinders.

small peak at $St_s = 0.011$ corresponds to the secondary frequency ($St = fd/U_0$, where St and f are Strouhal number and frequency, and subscripts 'p' and 's' refer to primary and secondary, respectively).

Similar flow behaviour is also noticed for $s/d = 1.3$. Kumar *et al.* (2008) termed this as quasi-periodic-I flow for a row of square cylinders, and the same terminology is retained here. Thus, *quasi-periodic-I* flow is obtained for $1.2 \leqslant s/d \leqslant 1.3$ and $Re = 100$, for in-line cylinders.

3.3. *Quasi-periodic-II flow* ($1.4 \leqslant s/d \leqslant 5$)

The instantaneous vorticity contours and streamlines for $s/d = 1.5$ and 4.0 are shown in figure 11. From figure 11(*a*) it is noticed that the vortex formed behind the first cylinder grows in the first gap. The presence of the second cylinder however interferes

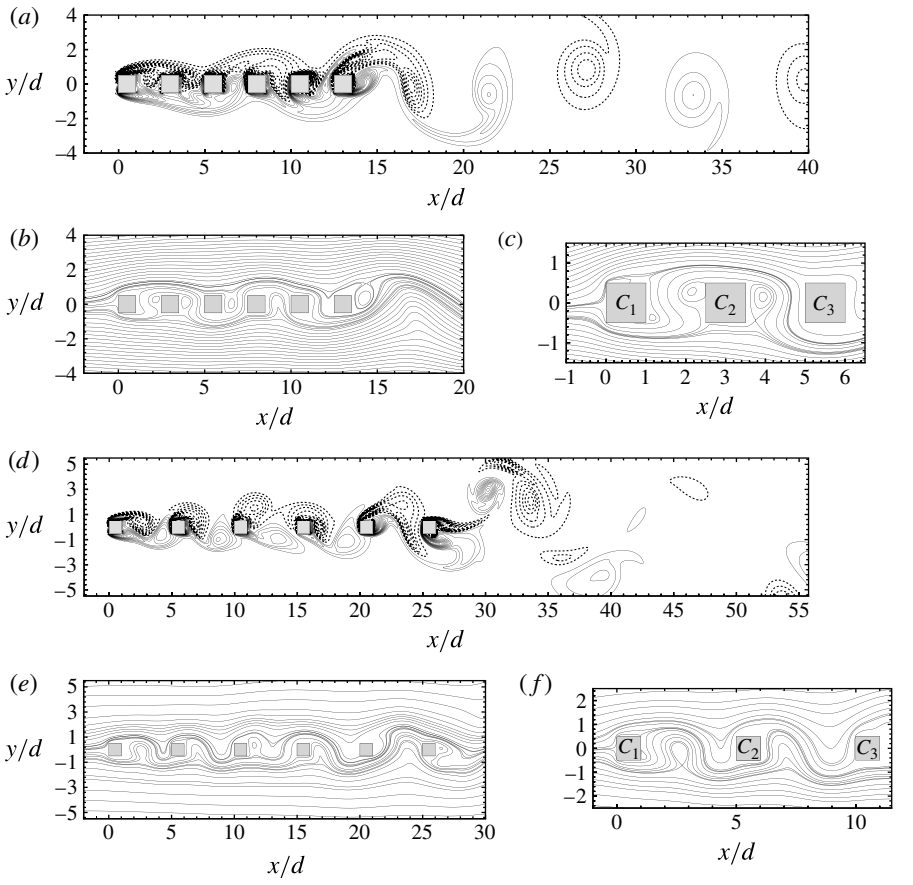

FIGURE 11. (*a,d*) Instantaneous vorticity contours, (*b,e*) streamlines, and (*c,f*) enlarged view of streamlines for (*a–c*) $s/d = 1.5$ and (*d–f*) $s/d = 4.0$ at $Re = 100$. The dashed lines in (*a,d*) indicate negative vorticity.

with this growing vortex thereby altering the nature of the forces experienced by both these cylinders. Similar interference phenomenon applies to other cylinders. This type of behaviour is noticed for $1.4 \leqslant s/d \leqslant 5$ at $Re = 100$ (see for example figure 11*d*).

The lift coefficient signal for all the cylinders at $s/d = 1.5$ is shown in figure 12, which indicates the presence of both primary and secondary frequencies. The time periods corresponding to both primary and secondary frequencies are variable in this regime; the variation is however less than 10 % of the mean value. This differentiates the present regime from the quasi-periodic-I flow of § 3.2. The C_L signal therefore suggests that the flow regime for $s/d = 1.5$ is *quasi-periodic-II* (Kumar *et al.* 2008), which is further confirmed from the C_D signals in figure 13. Notice that the modulations in the C_D signals have become more severe for larger spacings, which indicates that the contribution of the secondary frequency is more significant in the quasi-periodic-II flow. The power spectrum in figure 14 confirms that there exists a secondary cycle which spans over about four vortex shedding cycles. For $s/d = 1.5$ (figure 14*a*), the peak at $St_p = 0.082$ is the Strouhal number corresponding to the primary frequency and the peak shown in the inset (at $St_s = 0.02$) corresponds to

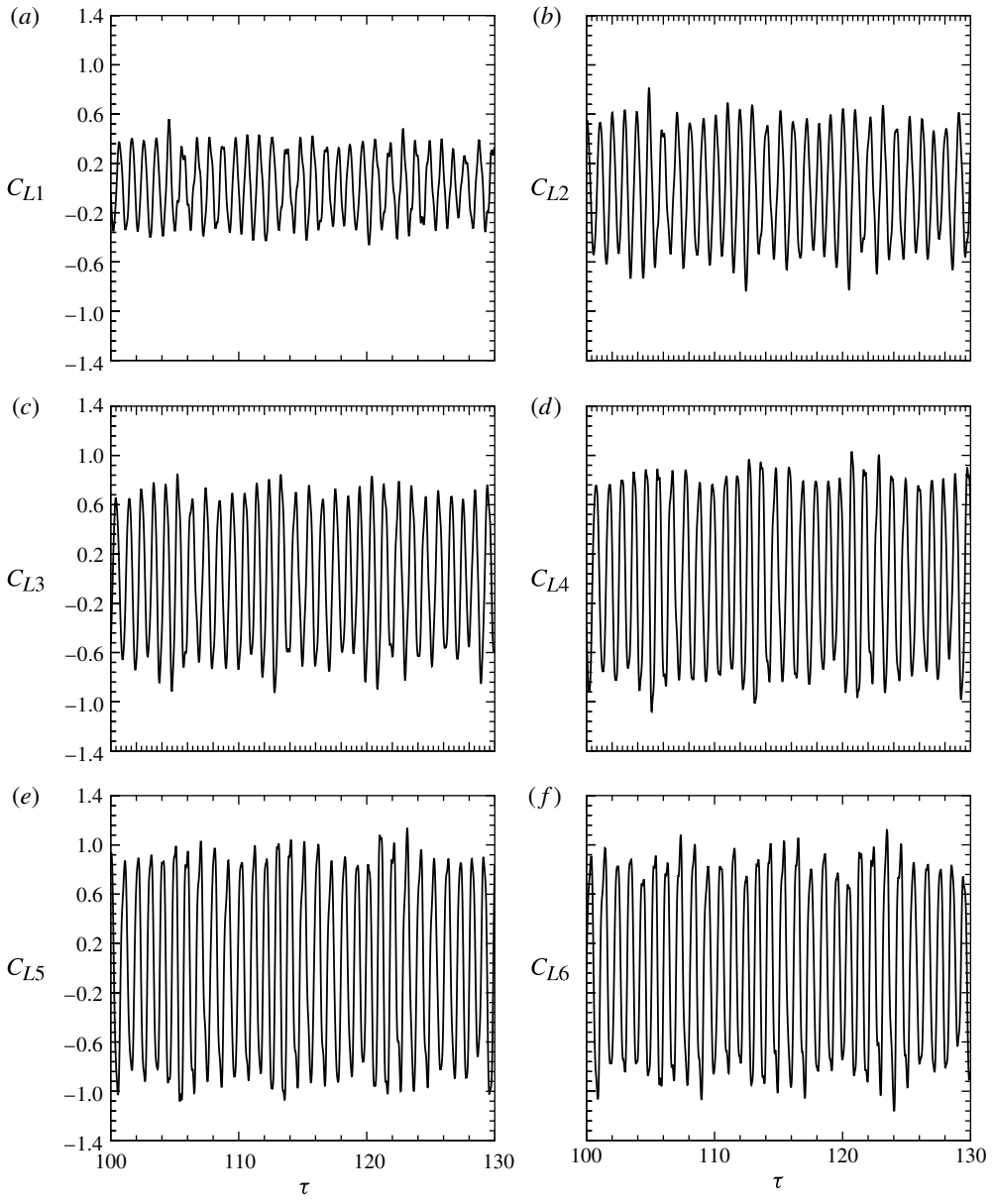

FIGURE 12. Time series of lift coefficient experienced by the cylinders at $s/d = 1.5$ and $Re = 100$.

the secondary frequency. The side peaks in figure 14 are due to variation in the time period of primary cycles. The flow is able to cross over to the other side of the cylinder more freely in this regime, as is apparent from the streamlines in figure 11(*b,c*), which leads to this secondary cycle. The presence of a secondary frequency is further strengthened from the power spectrum, where its magnitude is very small for $s/d = 1.5$ (figure 14*a*) but becomes comparable to the primary frequency at $s/d = 4.0$ (figure 14*b*). It is also noticed that the primary as well as

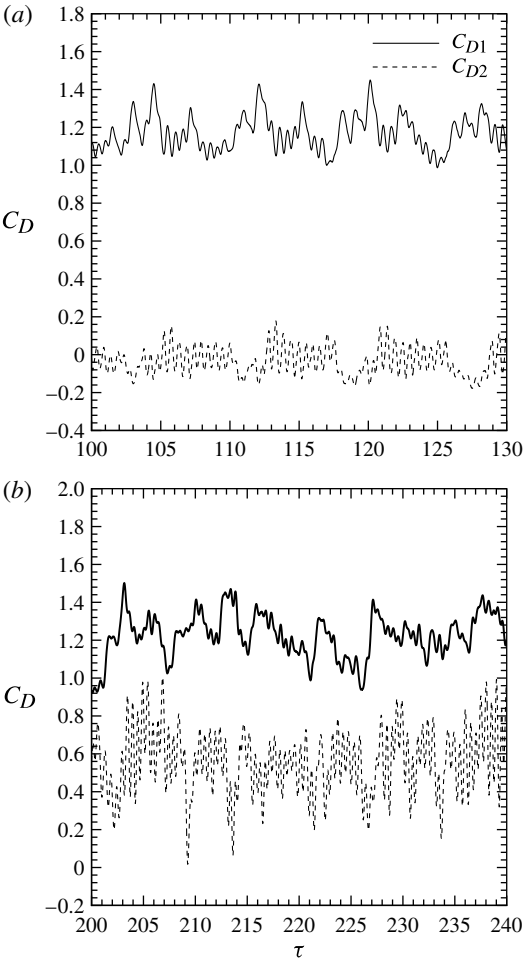

FIGURE 13. Time series of drag coefficient experienced by selected cylinders at (*a*) $s/d = 1.5$ and (*b*) $s/d = 4$ for $Re = 100$.

the secondary frequencies increase with an increase in the spacing, as shown later in figure 30. Thus, for spacing $1.4 \leqslant s/d \leqslant 5$, the flow is *quasi-periodic-II* in nature.

3.4. *Chaotic flow* ($6.0 \leqslant s/d \leqslant 10.0$)

The instantaneous vorticity contours at $s/d = 6.0$ and 10.0 are shown in figure 15. Notice that the computational domain has become very large along the streamwise direction, making the computations expensive. The vortices are shed in the gap between the cylinders and hit the downstream cylinder (figure 15*a,d*). The vortices from different downstream cylinders coalesce together. The location of vortices does not show any relationship among themselves as they move downstream, and the flow appears chaotic. The streamlines (figure 15*b,e*) indicate that flow can cross over to the other side of the cylinder. The signals of lift and drag coefficient for $s/d = 6.0$ are presented in figures 16 and 17, respectively. These signals confirm the chaotic nature of the flow. The power spectrum of C_L for $s/d = 6.0$ and 10.0 in figure 18 indicates the existence of a comparatively broad and continuous spectrum near St_s, characteristic

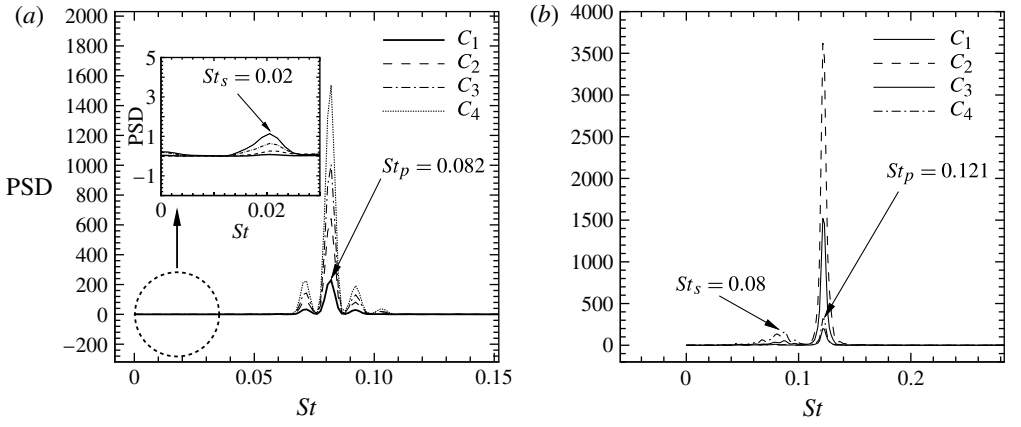

FIGURE 14. Power spectra of lift coefficients of selected cylinders at (*a*) $s/d = 1.5$ and (*b*) $s/d = 4.0$ for $Re = 100$. The inset in (*a*) is provided to show the secondary frequency clearly.

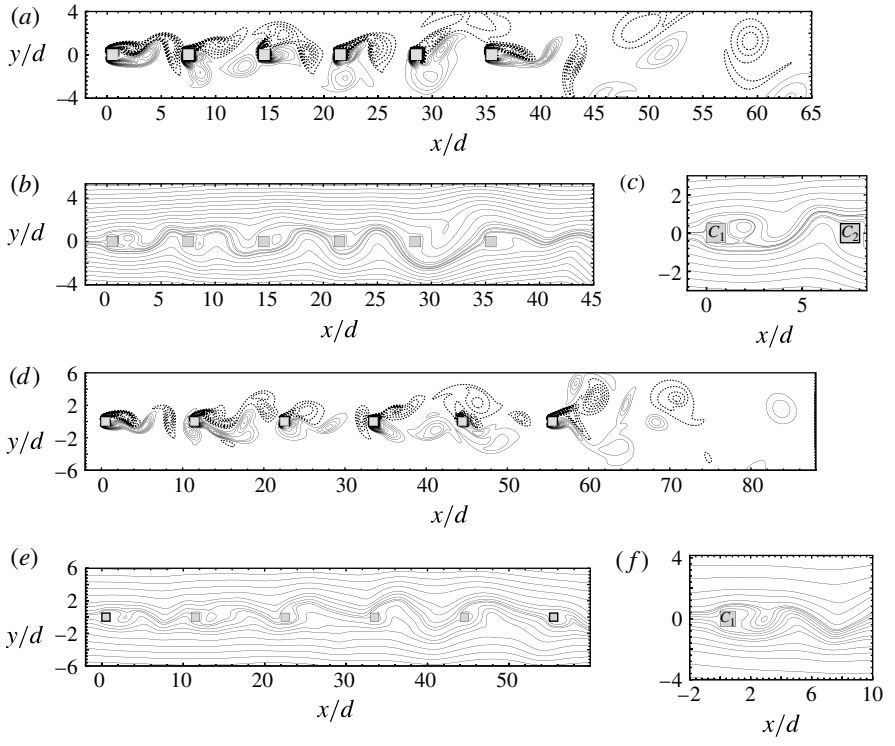

FIGURE 15. (*a,d*) Instantaneous vorticity contours, (*b,e*) streamlines, and (*c,f*) enlarged view of streamlines for (*a–c*) $s/d = 6.0$ and (*d–f*) $s/d = 10.0$ at $Re = 100$. The dashed lines in (*a,d*) indicate negative vorticity.

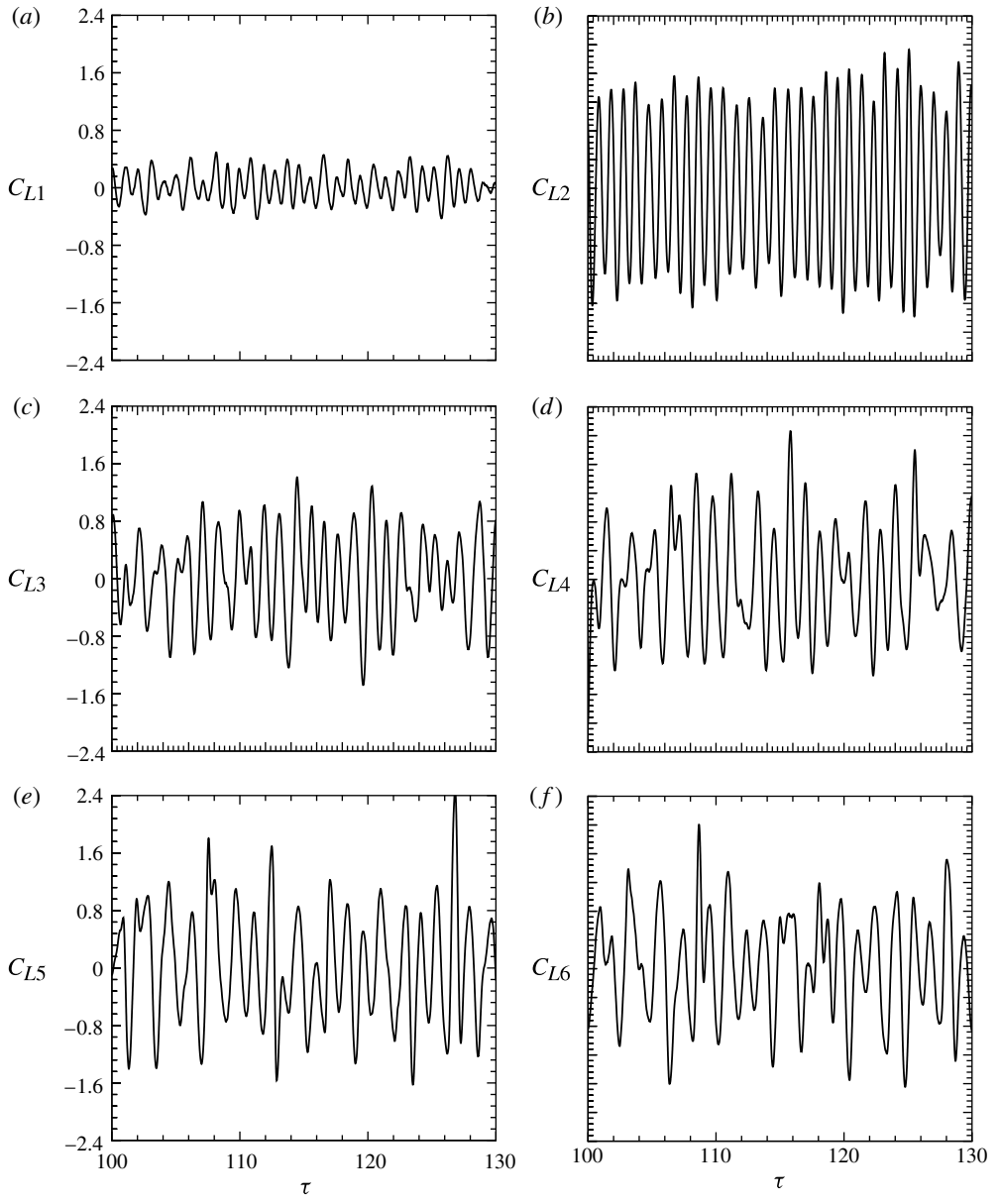

FIGURE 16. Time series of lift coefficient experienced by the cylinders at $s/d = 6.0$ and $Re = 100$.

of chaotic flows. Furthermore, the magnitude of the secondary frequency ($St_s = 0.08$ for $s/d = 6.0$ and $St_s = 0.1$ for $s/d = 10.0$) is comparatively large and it appears more prominently in the power spectra as compared to the aforementioned flow regimes.

The vortices shed by the cylinders at larger spacing are relatively strong as these are fully grown vortices. Therefore, when these vortices interfere with the downstream cylinders, variation in forces occurs due to a combination of vortex shedding from the cylinder and interference by vortices shed from the upstream cylinder, leading to

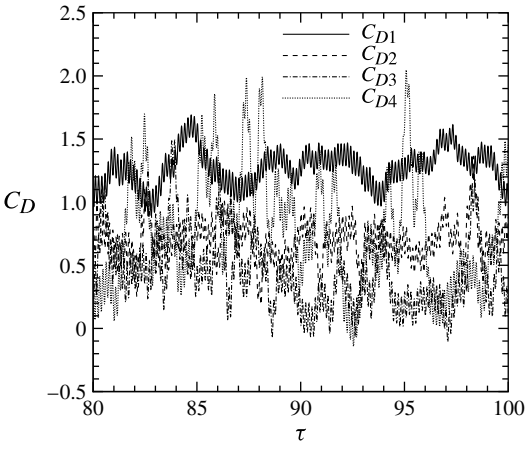

FIGURE 17. Time series of drag coefficient experienced by selected cylinders at $s/d = 6.0$ for $Re = 100$.

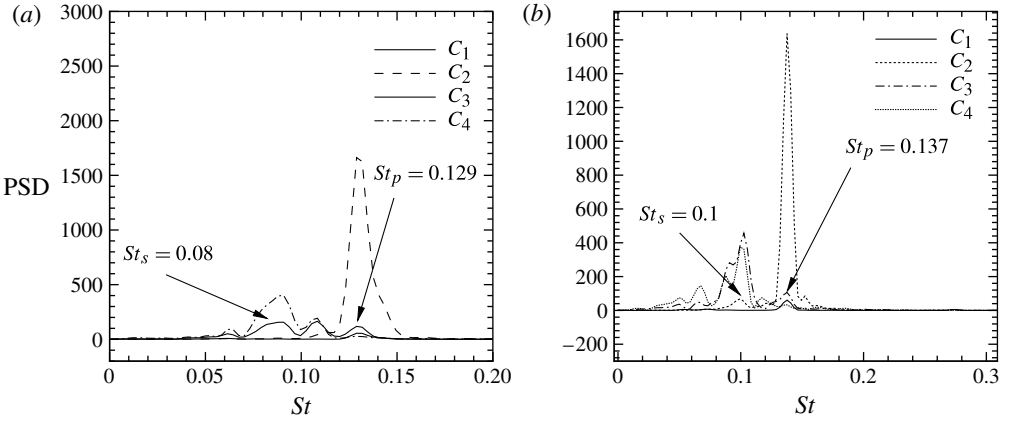

FIGURE 18. Power spectra of lift coefficients of selected cylinders at (*a*) $s/d = 6.0$ and (*b*) $s/d = 10.0$ for $Re = 100$.

chaotic flow behaviour. Similar behaviour is also noticed for other spacings in the range of $6.0 \leqslant s/d \leqslant 10$. Thus, the flow is *chaotic* for $s/d \geqslant 6.0$ at $Re = 100$.

4. Comparison of the flow regimes with experimental results

The objective of this section is to experimentally confirm the numerically obtained flow patterns. Flow visualization and the PIV technique are used for this purpose. The flow patterns for different spacings at $Re = 100$ obtained by these techniques are presented in figures 19 and 20. The vorticity field is obtained from the velocity field measured using PIV. In each figure, the flow direction is from left to right and the contour lines are for instantaneous vorticity.

Similar to numerical investigation, experimental data also indicate a single wake behind all the cylinders at $s/d = 0.5$ and 1.0 (compare figures 19*a,b* and 20*a,b* with figure 3*a,d*, respectively). This confirms the synchronous nature of the flow

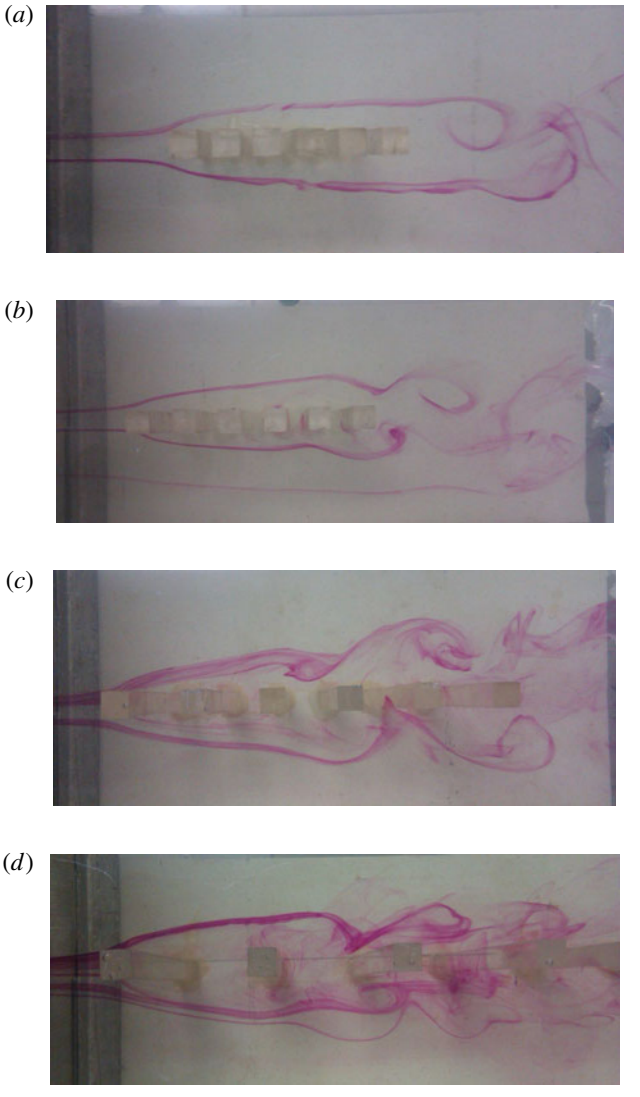

FIGURE 19. (Colour online) Flow visualization for (*a*) $s/d = 0.5$, (*b*) $s/d = 1.0$, (*c*) $s/d = 2.0$ and (*d*) $s/d = 4.0$ at $Re = 100$.

at small spacings. The formation of a shear layer starting at the first cylinder and the shedding of a vortex from the last cylinder are evident from figures 19(*a,b*) and 20(*a,b*). Figure 20(*c*) shows (for $s/d = 2.0$ at $Re = 100$) the growth of vortices between the gaps and their subsequent interference with the downstream cylinders. The interference by the cylinders alters the pressure distribution around the cylinders, which leads to quasi-periodic-II type of flow behaviour. Similar flow behaviour is also noticed for $s/d = 4.0$ as shown in figure 20(*d*); this latter figure can be compared with figure 11(*d*). Similar comparison with experimental results was done at $s/d = 0.5$, 1.0 2.0 and 4.0 with $Re = 150$ (not shown).

The normalized time-averaged streamwise velocity along two lateral locations is presented in figure 21 (between the second and third cylinders and at a distance of

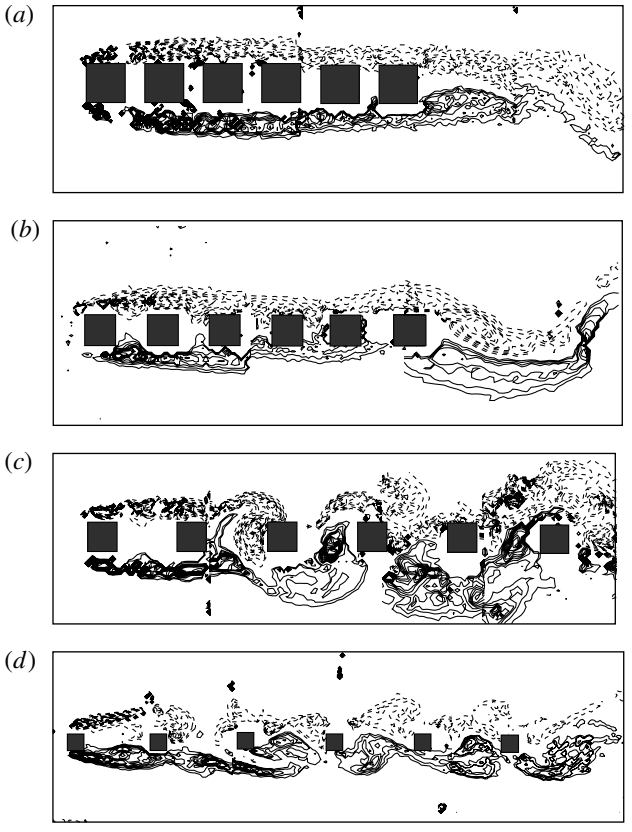

FIGURE 20. Experimentally obtained vorticity contours for (*a*) $s/d = 0.5$, (*b*) $s/d = 1.0$, (*c*) $s/d = 2.0$ and (*d*) $s/d = 4.0$ at $Re = 100$.

$3d$ from the last cylinder) and figure 22 (between the third and fourth cylinders and at a distance of $3d$ from the last cylinder), for $s/d = 2.0$ and 4.0 and $Re = 100$ and 150. Good quantitative agreement between experimental and numerical results is demonstrated by these figures. Such comparison helps establish confidence in the proposition of the various flow regimes outlined in § 3.

5. Effect of Reynolds number on the flow regimes

To understand the effect of Reynolds number on the flow regimes and flow parameters, simulations are further carried out for $Re =$ 40, 60, 80 120, 140, 150 and 160 (table 1). The lower limit of Re is set at 40, which is above the critical Reynolds number for vortex shedding. The upper limit (of $Re = 160$) is decided in view of the constraint of two-dimensionality (Saha, Biswas & Muralidhar 2003; those results are however for a single square cylinder). During PIV experiments it was noticed that PIV particles remain in the illumination plane (which was greater than 20 times the cylinder diameter in the streamwise direction); this preliminary observation suggests that the flow is indeed two-dimensional for $Re \leqslant 150$. Besides $Re = 100$, the experiments at $Re = 150$ provide confirmation of the results mentioned earlier. The experiments have been further extended to $Re = 320$ to explore the flow behaviour at still higher Reynolds numbers (table 1). The combined results of numerical and

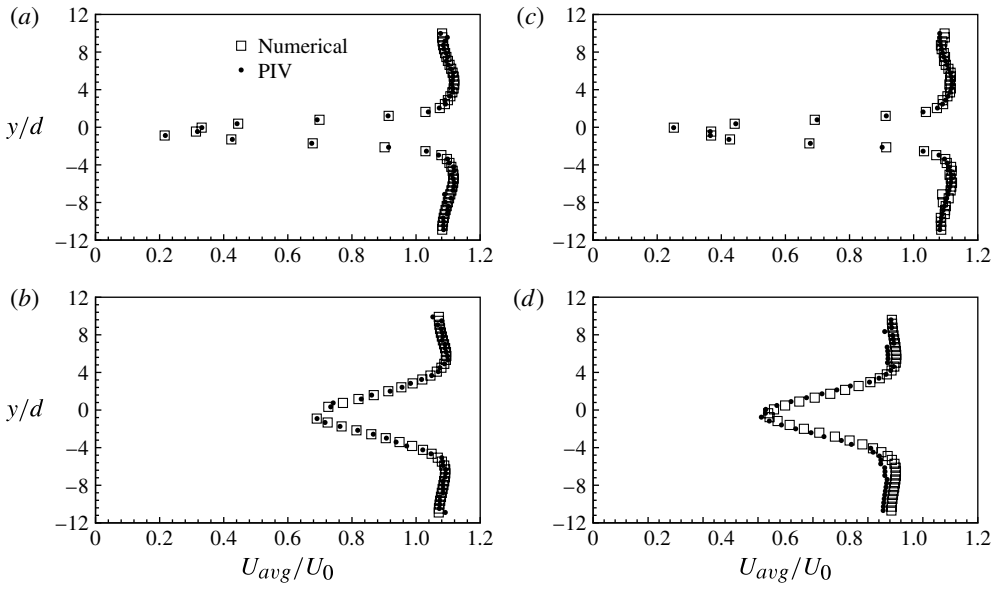

FIGURE 21. Comparison of numerical and experimental data for normalized time-averaged streamwise velocity profiles at two locations: (*a,c*) between the second and third cylinders, and (*b,d*) at 3*d* downstream of the last cylinder. Note that these are for $Re = 100$ and two spacings: (*a,b*) $s/d = 2$ and (*c,d*) $s/d = 4.0$.

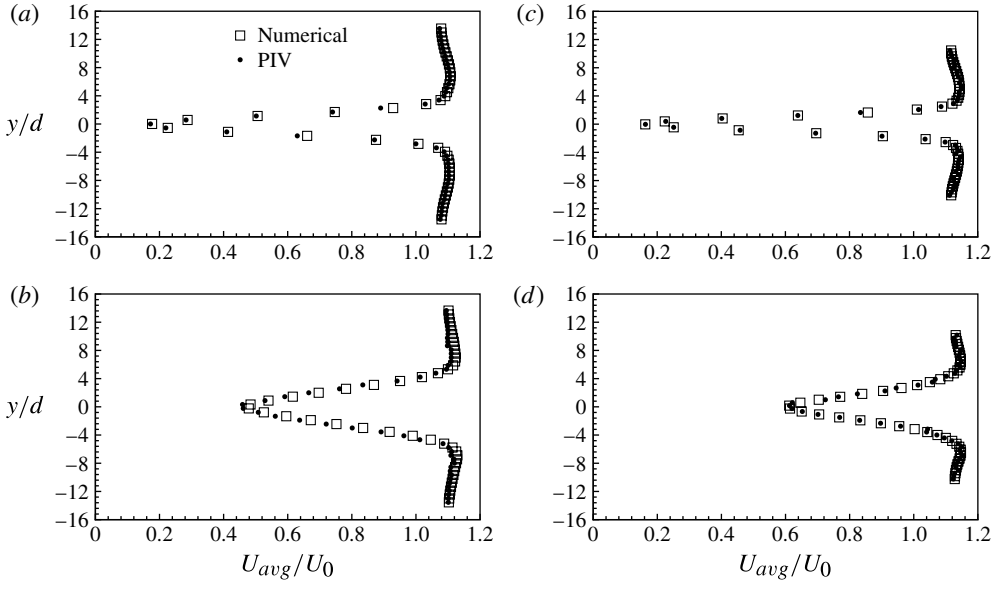

FIGURE 22. Comparison of numerical and experimental data for normalized time-averaged streamwise velocity profiles at two locations: (*a,c*) between the third and fourth cylinders, and (*b,d*) at 3*d* downstream of the last cylinder. Note that these are for $Re = 150$ and two spacings: (*a,b*) $s/d = 2$ and (*c,d*) $s/d = 4.0$.

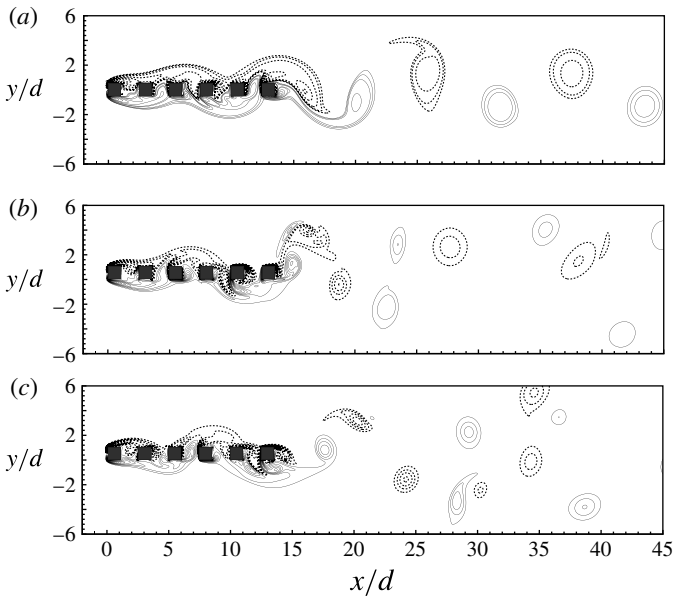

FIGURE 23. Instantaneous vorticity contours for (*a*) $Re = 60$, (*b*) $Re = 120$ and (*c*) $Re = 160$ at $s/d = 1.5$. The dashed lines indicate negative vorticity.

experimental investigations are used to propose a flow regime map in terms of non-dimensional spacing and Reynolds number, as described in the next section.

Instantaneous vorticity contours for $Re = 60$, 120 and 160 at $s/d = 1.5$ are shown in figure 23 and the corresponding signals for the lift coefficient are presented in figures 24–26. The effect of increasing Reynolds number is clearly visible from these figures. It is noticed that with an increase in the Reynolds number for a given spacing the flow transits from synchronous (figure 24) to quasi-periodic-I (figure 25) and further to quasi-periodic-II (figure 26).

Figure 27 shows instantaneous vorticity contours for $Re = 80$, 120 and 160 at $s/d = 3.0$. The vortices shed from the upstream cylinders travel in the gap between the cylinders and subsequently interfere with the downstream cylinders. It is noticed from the time series and power spectra (not shown) that the flow is quasi-periodic-I in nature for $Re = 80$ and quasi-periodic-II for other Reynolds numbers. With further increase in the spacing beyond $s/d = 6.0$, it has been noticed that the flow changes to chaotic irrespective of the Reynolds number.

The instantaneous vorticity contours for $s/d = 0.5$, 1.0 and 2.0 at $Re = 320$, obtained *experimentally*, are shown in figure 28. It is expected that three-dimensional effects will occur at such a high Reynolds number. Interestingly, the essential flow phenomenon observed at lower Reynolds number is also visible at this Reynolds number; the transitions from synchronous to chaotic through quasi-periodic-I or quasi-periodic-II, however, cannot be clearly spelled out from the data. For low spacing ($s/d = 0.5$), the vortices do not flow between the gaps; they rather interfere with the bottom or top side of the corresponding downstream cylinder. At larger spacings, the vortices are affected by the top, bottom and front sides of the cylinders. This leads to either quasi-periodic-II or chaotic flow behaviour depending upon the frequency of interference of the vortices. Thus, the results obtained at low Reynolds number may form the basis for prediction of flow phenomenon at higher Reynolds numbers.

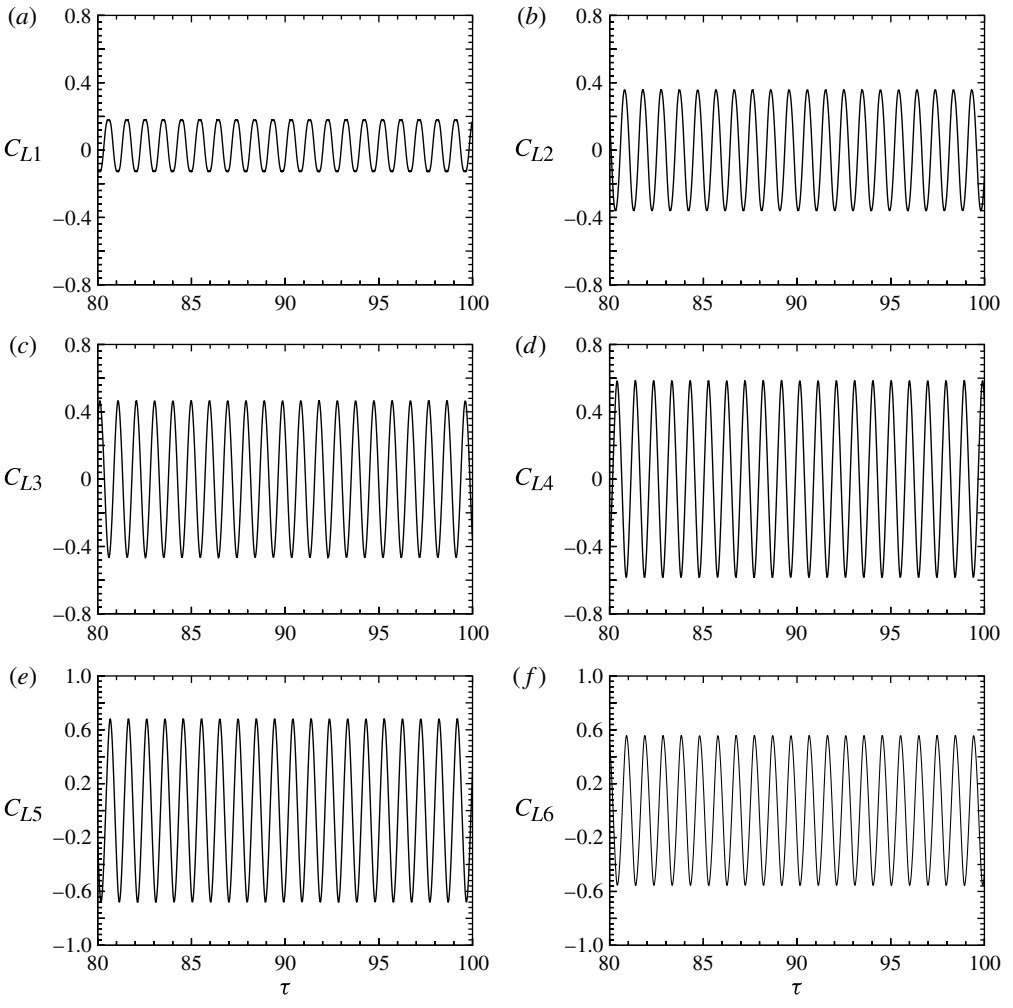

FIGURE 24. Time series of lift coefficient experienced by the cylinders at $s/d = 1.5$ and $Re = 60$.

For in-line cylinders the effect of Reynolds number is opposite to that of the case of flow across a row of side-by-side cylinders. In the latter case, for a given spacing with an increase in the Reynolds number, the flow transits from chaotic to synchronous through quasi-periodic-II and quasi-periodic-I regimes (Sewatkar *et al.* 2009). The other difference of the Reynolds number is that in the case of a row of cylinders the transitions are more prominently noticed at larger spacings ($s/d = 3.0$ and 4.0), while in the case of in-line cylinders the transitions are predominant at lower spacings ($s/d \leqslant 1.5$).

6. Flow regime map

The flow regimes have been approximately demarcated based on the vorticity contours, time series of drag and lift coefficients, and power spectra, at different spacings and Reynolds numbers. As seen from figure 29, there exists synchronous,

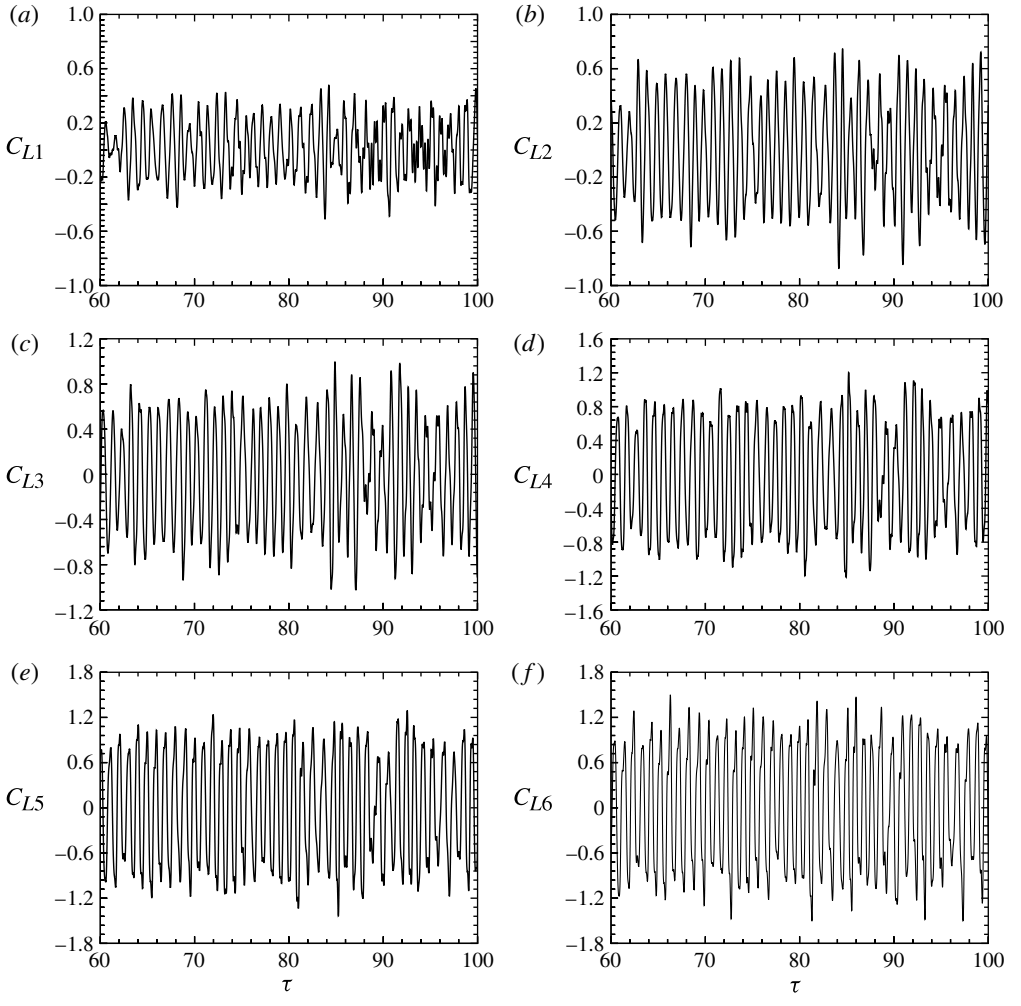

FIGURE 25. Time series of lift coefficient experienced by the cylinders at $s/d = 1.5$ and $Re = 120$.

quasi-periodic-I, quasi-periodic-II, and chaotic flow regimes for $0 \leqslant s/d \leqslant 6.0$ and $40 \leqslant Re \leqslant 160$. The limiting case of $s/d = 0$ (single bluff body of large aspect ratio placed parallel to the flow) is also considered. The flow is synchronous for all Reynolds numbers at $s/d = 0$ because the cylinders behave like a single bluff body.

The figure depicts synchronous flow at smaller Re and lower s/d. This is opposite to the case of flow across a row of cylinders, where synchronous flow is noticed at higher Re and larger s/d (Sewatkar *et al.* 2009). A quasi-periodic-I flow regime with a variable time period of primary cycles but constant time period for secondary cycles occurs over a small range of spacings and Reynolds number. The transition from synchronous to quasi-periodic-II via quasi-periodic-I is noticed for $Re \leqslant 100$ only (except $Re = 80$), beyond which the synchronous flow transits directly to quasi-periodic-II. Alternatively, the spacing range is so small that the quasi-periodic-I regime has not been resolved in those simulations. The secondary frequency overwhelms the primary frequency giving rise to the chaotic behaviour. The flow is chaotic at larger

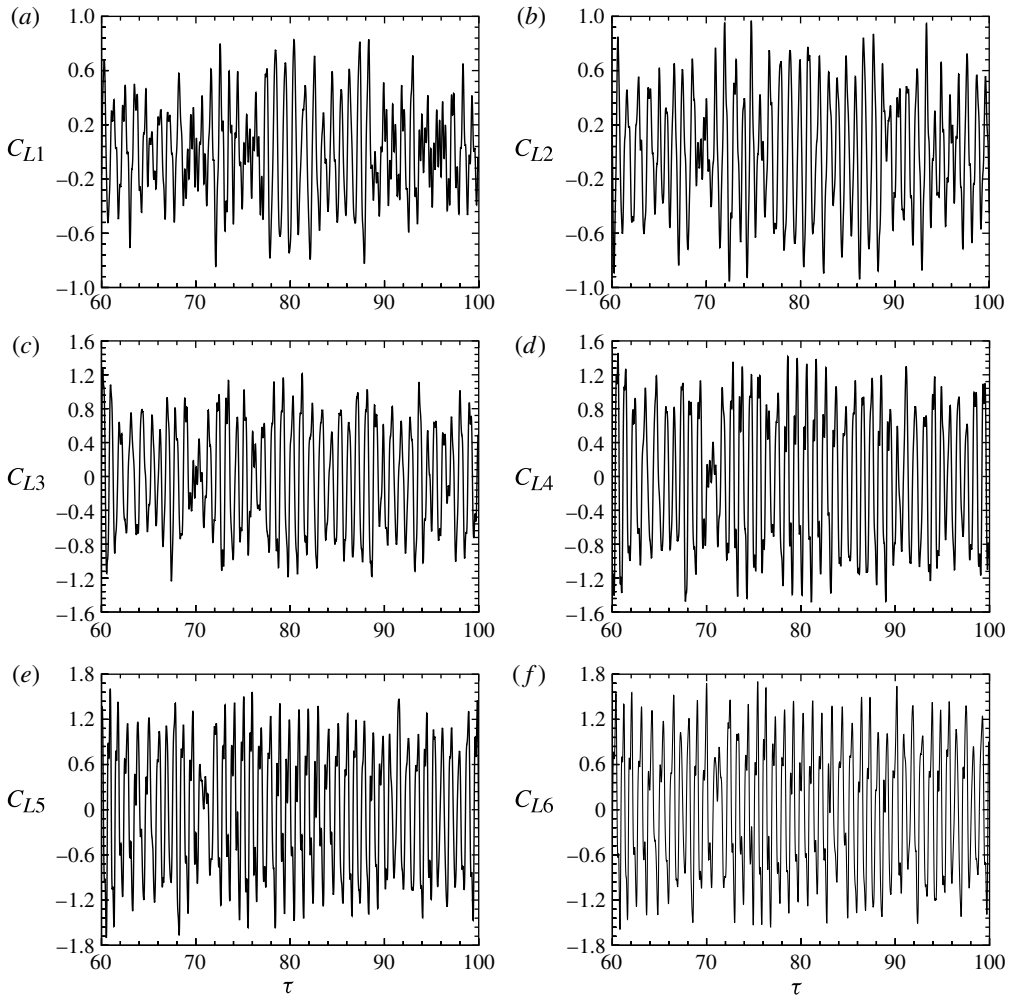

FIGURE 26. Time series of lift coefficient experienced by the cylinders at $s/d = 1.5$ and $Re = 160$.

spacings and higher Reynolds number, as is evident from the figure. The flow with a broader spectrum near the secondary frequency confirms the chaotic nature of the flow for $6.0 \leqslant s/d \leqslant 10.0$. It is evident that the flow around multiple in-line cylinders tends to have a quasi-periodic-II nature.

For comparison, Liang *et al.* (2009) for six circular cylinders at $Re = 100$ noticed that the instantaneous flow patterns for $s/d = 2.6$ reveal an antisymmetric vortex shedding activity, i.e. there is a 180° phase difference from one cylinder to the next, and during one period the vortices travel a distance twice the cylinder spacing. For $s/d = 3.0$, the vortices become much weaker, the strong antisymmetry disappears, and the vortex motion is no longer synchronized with the spacing, leading to reduced r.m.s. forces. Our results are consistent with these observations. Further, in accordance with the earlier observation of Liang *et al.* (2009), it was noticed that the vortex shedding starts from the last cylinder and proceeds upstream.

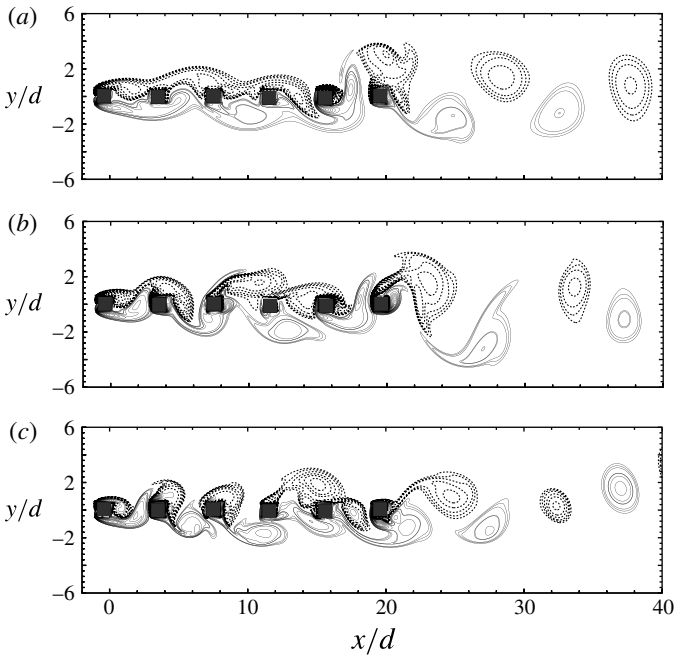

FIGURE 27. Instantaneous vorticity contours for (*a*) $Re = 80$, (*b*) $Re = 120$ and (*c*) $Re = 160$ at $s/d = 3.0$. The dashed lines indicate negative vorticity.

7. Flow parameters

Variation of flow parameters such as Strouhal number, lift and drag coefficients for different cylinders at various spacings is presented in this section.

7.1. *Strouhal number*

Referring back to figure 6, which shows the power spectra of different cylinders for $s/d = 0.5$ and $Re = 100$, it is noticed that the dominant frequency is identical for all the cylinders. A similar observation applies to all other spacings and Reynolds numbers investigated herein. It is therefore argued that the vortex shedding of the upstream cylinders locks with the vortex shedding frequency of the downstream cylinders. A careful observation of the signal shows that the shedding from one cylinder has a definite relationship with shedding from any other cylinder, although the shedding between two adjacent cylinders is out of phase, except for the last two cylinders for which it is in phase. Sakemoto *et al.* (1987) reported that the vortex shedding frequencies of two in-line square cylinders are the same for $s/d < 14$, but two distinct frequencies of two cylinders are noticed for $s/d > 14$. Xu & Zhou (2004) in their experimental work with two in-line circular cylinders argued that the near wake generated by the upstream cylinder (which could be considered as an oscillating flow) interferes and influences the vortex shedding from the downstream cylinder. The two vortex shedding processes therefore influence each other, resulting in the lock-on phenomenon. The present result, while being in qualitative agreement with results for two in-line cylinders, further demonstrates that this lock-on phenomenon extends to a larger number of in-line cylinders. The vortex shedding frequency in all the cases

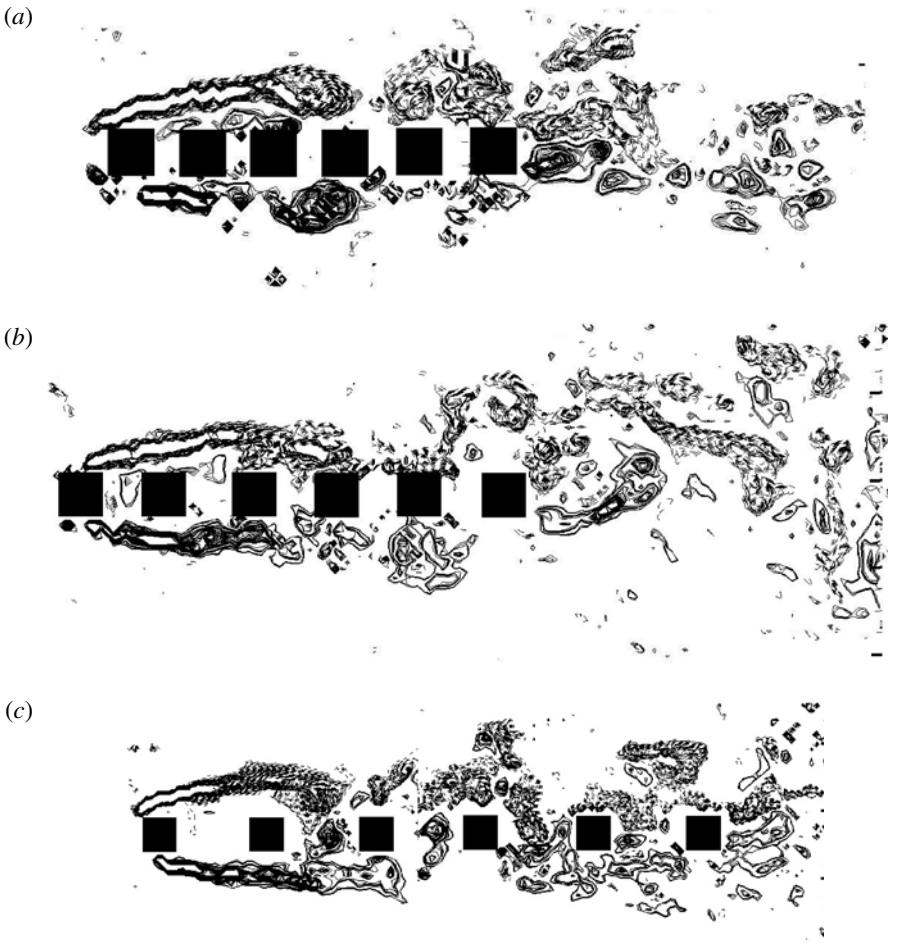

FIGURE 28. Experimentally obtained instantaneous vorticity contours for $Re = 320$ at (*a*) $s/d = 0.5$, (*b*) $s/d = 1.0$ and (*c*) $s/d = 2.0$.

is however much smaller than that of an isolated cylinder ($St = 0.148$ at $Re = 100$; Sharma & Eswaran 2004), shown in figure 30(*a*).

For $s/d = 0.5$, the shear layer passes over the downstream cylinders without rolling (figure 3*a*). The cylinders therefore act as a single body with a large aspect ratio, which leads to a smaller St_p as compared to an isolated cylinder. As the spacing is increased to $s/d = 1$, St_p suddenly drops to 0.07, which is almost half that for an isolated cylinder. In this case, the shear layer moves into the gaps between the cylinders without rolling, which renders additional stability to the flow (figure 3*d*). This causes the St_p to reduce drastically as the flow is retarded. The physical description offered by Xu & Zhou (2004) for flow retardation in the context of two in-line circular cylinders is recalled here. They argued that the shear layers separating from the upstream cylinder reattach on the upstream side of the downstream cylinder and then separate, perhaps joining the shear layers around the downstream cylinder, to form vortices behind the downstream cylinder. Nevertheless, the shear layer impingement upon the downstream cylinder and interactions between the shear

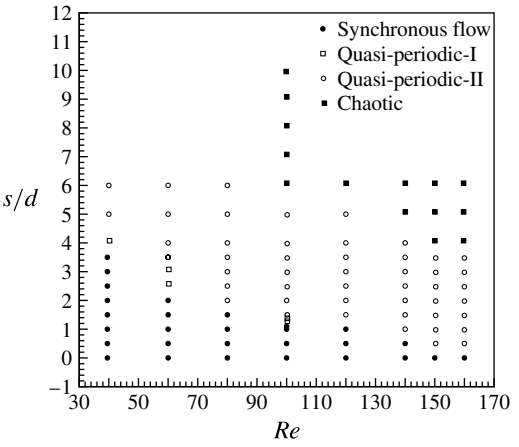

FIGURE 29. Flow regime map at various Reynolds numbers and spacings. Note that the position of the symbols indicates the discrete values of the spacing and Reynolds number at which the simulations have been carried out. Notice that the range of spacing for the synchronous regime increases with a decrease in Re.

layers originating from different cylinders may have an influence on the vortex shedding frequency, contributing to the decrease in the corresponding Strouhal number. Beyond $s/d > 1.0$, St_p increases rapidly and reaches a value of 0.122 at $s/d = 4.0$ and $Re = 100$ (figure 30*a*). This is due to the commencement of vortex shedding from upstream cylinders. With a further increase in the spacing ($s/d \geqslant 5$), St_p increases rather slowly. Similar variation is noticed for all Reynolds numbers considered in the present work (figure 30*b*); however, the Strouhal number is in general higher for larger Reynolds number. In particular, the large dip in the St_p at $s/d = 1.0$ is noted for all Reynolds numbers.

The secondary frequency appears for the first time at $s/d = 1.2$ with $Re = 100$, beyond which it increases with an increase in the spacing (figure 30*a*). The secondary frequency appears in the signal due to the wake interference. For $1.5 \leqslant s/d \leqslant 4.0$, the vortices grow in the gap between the cylinders and interfere with the downstream cylinder before shedding. For $s/d > 4.0$, the vortices interfere with the downstream cylinders after shedding. This causes changes in the pressure distribution of the wake, which leads to the dominant appearance of the secondary frequency.

7.2. *Drag and lift coefficients*

The drag and lift coefficients were the major concern of the researchers in the case of two in-line cylinders because these quantities showed abrupt changes in the magnitude near $s/d = 2.5$ (Mizushima & Suehiro 2005). The variation of mean drag and r.m.s. lift coefficients with spacing for all the six cylinders is shown in figures 31 and 32, respectively. These results were calculated at $Re = 100$; approximately similar behaviour is noticed at other Reynolds numbers. The mean drag experienced by any of the cylinders and at any spacing is smaller than the mean drag for an isolated cylinder (Sharma & Eswaran 2004), indicated by a dashed line in figure 31.

The mean drag on the first cylinder at about $C_{Dmean} = 1.2$ is almost unaffected by the spacing (figure 31*a*). The drag on the second cylinder attains a negative value for $s/d \leqslant 2$ and increases monotonically with spacing (figure 31*b*). Negative drag has been reported in the literature for the two-cylinder case for the same range of

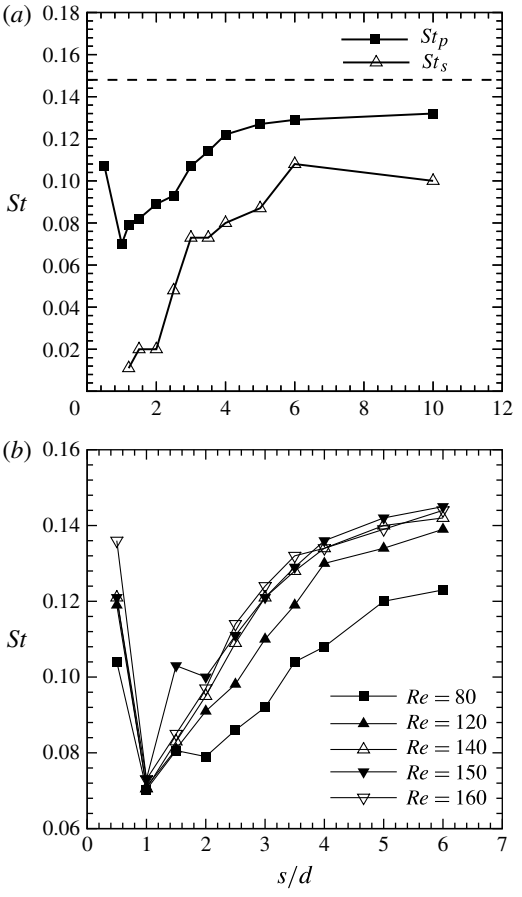

FIGURE 30. Variation of Strouhal number with spacing, corresponding to (*a*) primary and secondary frequencies for $Re = 100$ and (*b*) the primary frequency at other Reynolds numbers. Note that the Strouhal numbers for all the cylinders at a particular spacing are equal. The dashed line in (*a*) indicates the Strouhal number for an isolated cylinder at $Re = 100$ (Sharma & Eswaran 2004).

parameters (Zdravkovich 1987; Meneghini *et al.* 2001). The fact that the second cylinder is completely submerged within the wake of the first cylinder causes the mean drag to be negative at smaller spacings. The third to sixth cylinders show non-monotonic behaviour of the mean drag coefficient with spacing. Each of these cylinders experiences a sharp drop in mean drag at a certain spacing: for the third cylinder the mean drag suddenly drops beyond $s/d = 3$ (figure 31*c*), for the fourth it drops beyond $s/d = 2.5$ (figure 31*d*) and for the fifth and sixth cylinders it drops beyond $s/d = 2$ (figure 31*e*,*f*). Beyond each of the above-mentioned spacings the flow pattern around the cylinders changes, although the *quasi-periodic* nature of the overall flow is retained. For example at $s/d = 4$, the third cylinder actually starts shedding vortices (figure 11*d*), which causes a drop in the drag coefficient. Similar behaviour is also noticed for the other cylinders beyond the respective spacings mentioned above. As the spacing increases beyond these values, the drag increases and attains a value of $C_{Dmean} \approx 0.8$ for all cylinders except the first. These results are qualitatively consistent with the earlier experimental results for two in-line cylinders. In order to obtain

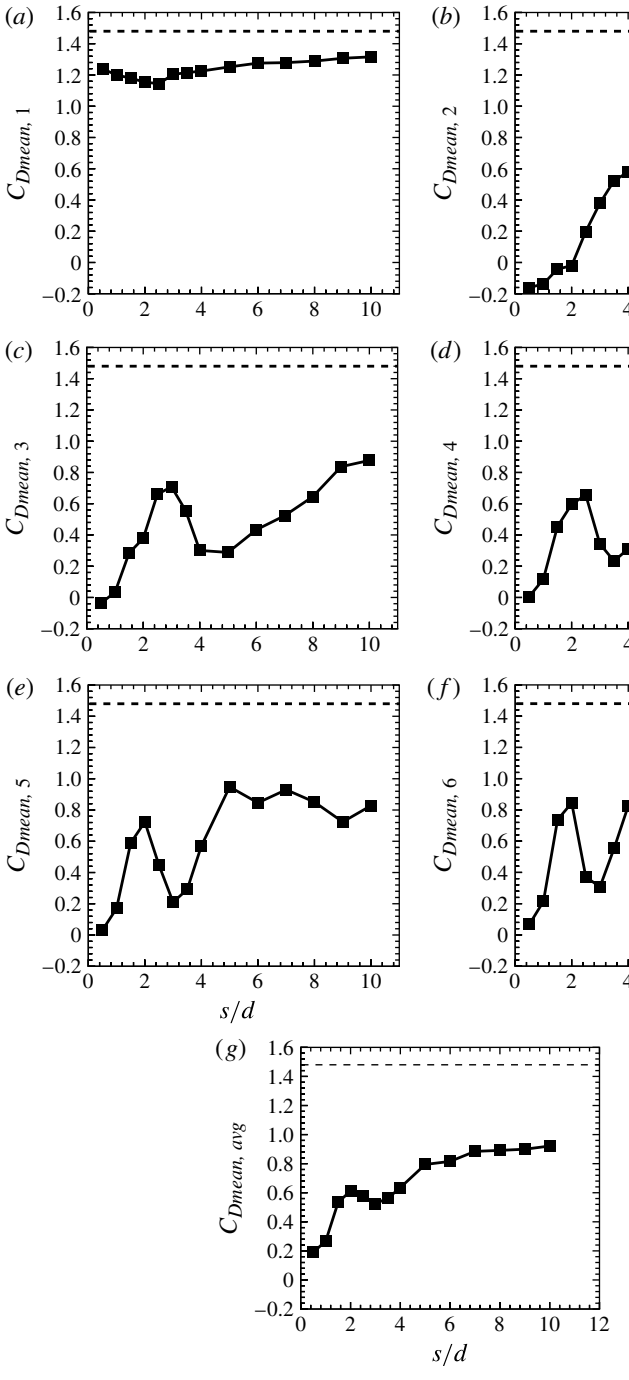

FIGURE 31. (*a–f*) Mean drag coefficient experienced by the cylinders and (*g*) average mean drag coefficient per cylinder as a function of spacing for $Re = 100$. The dashed line indicates the drag coefficient for an isolated cylinder at $Re = 100$ (from Sharma & Eswaran 2004).

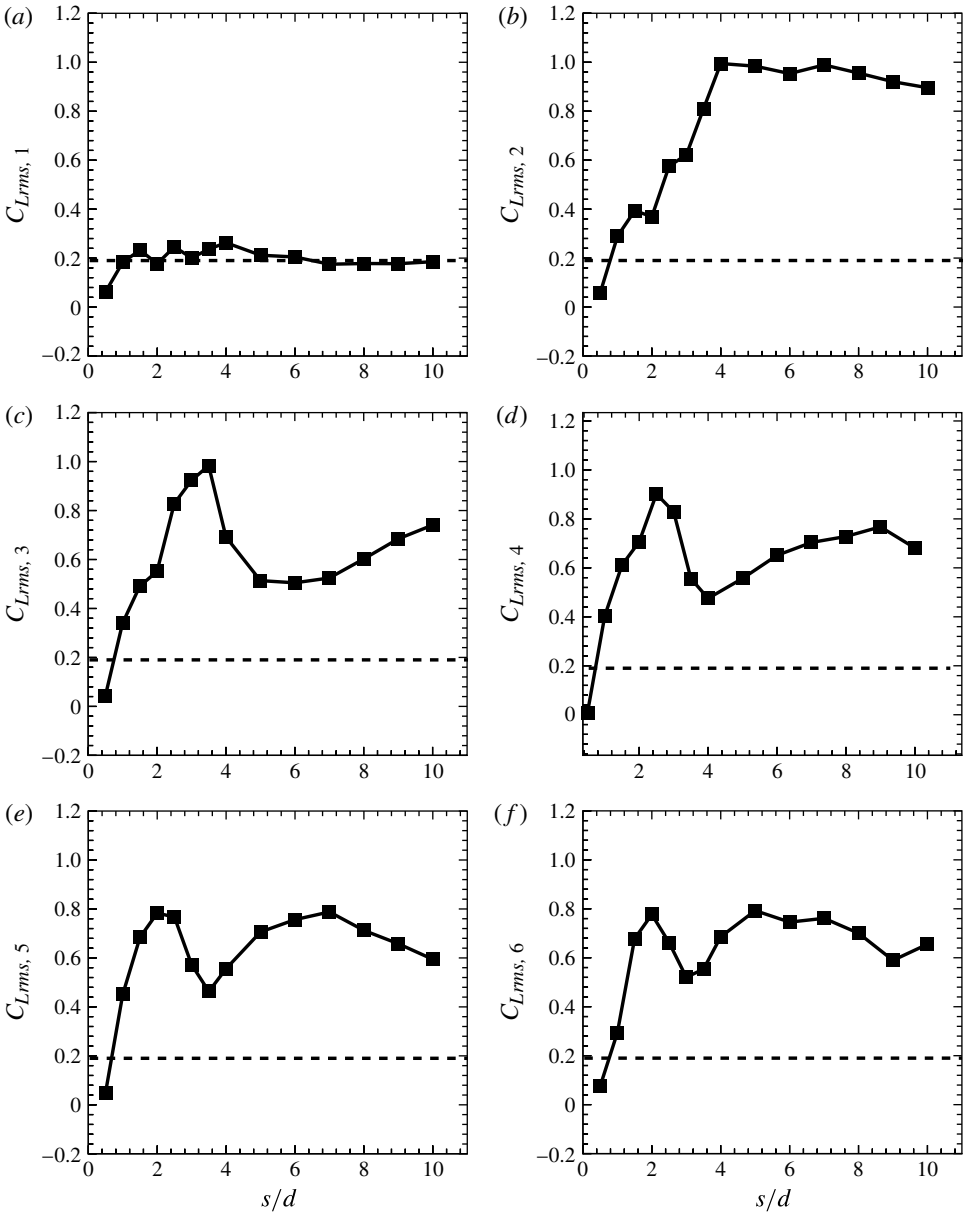

FIGURE 32. Root mean square lift coefficient experienced by the cylinders as a function of spacing for $Re = 100$. The dashed line indicates the r.m.s. lift coefficient for an isolated cylinder at $Re = 100$ (from Sharma & Eswaran 2004).

information on the overall flow behaviour, the average value of mean drag coefficient per cylinder ($C_{Dmean,\,avg}$) was computed and plotted in figure 31(*g*). The average drag more or less increases monotonically (other than a small dip at $s/d = 3.0$) from 0.20 to 0.92.

The lift coefficient experienced by the cylinders varies periodically with time for the Reynolds number considered in the present work. However, its value averaged over a

large number of cycles is zero. Therefore, the variation of root mean square value of lift coefficient (C_{Lrms}) with spacing is plotted at $Re = 100$, as shown in figure 32. The value of C_{Lrms} on the first cylinder remains close to the value for an isolated cylinder ($C_{Lrms} = 0.19$), as is evident from figure 32(*a*). For the second cylinder, figure 32(*b*) shows that the r.m.s. lift exhibits a single maximum at around $s/d = 3$–4. However, C_{Lrms} for the third to sixth cylinders in figure 32(*c–f*) shows an abrupt drop at about $s/d = 3.0$–4.0. The location of the dip correlates with the dip observed in the mean drag coefficient discussed above. A much larger value ($C_{Lrms} = 1.0$) for the second and third cylinders is noted at around $s/d = 3.5$ (figure 32*b,c*), which suggests that r.m.s. lift can be larger than mean drag on the cylinders. Also, notice that C_{Lrms} is particularly small at small spacing ($s/d = 0.5$) for all the cylinders.

8. Wake interference and its effect on flow parameters

The aim of this section is to elucidate the wake interference mechanism and its effect on the flow parameters such as drag and lift coefficients. It is argued that the distance at which the wake is affected by the downstream cylinder would govern the transition between the flow regimes. Figure 33 presents the instantaneous wakes behind the cylinders with $s/d = 1.0$, 1.2, 4.0 and 6.0 at $Re = 100$. Here the wake is defined as the region behind the cylinder where the instantaneous streamwise velocity is less than the free-stream velocity. For $s/d = 1.0$, figure 33(*a*) shows that the cylinders are enveloped in a single wake and the wake is structured in the downstream region. Owing to the small gap between the cylinders (figure 3) the convection in the gap is negligible as compared to diffusion. This is also attributed to the fact that the local Reynolds number is small due to the small local length scale for low spacing. Thus, the vorticity generated in the gap is diffused away without vortex shedding. When the downstream cylinder is placed very close to the upstream cylinder, the wake structure of the upstream cylinder is not altered substantially, because immediately behind the upstream cylinder the streamwise velocity is either close to zero or negative. This is similar to the single-cylinder case, where obviously there is no interference. Thus, the wake formed by closely spaced cylinders is similar to that of a single cylinder, which leads to the sinusoidal nature of the lift coefficient signal and a synchronous flow.

At $s/d = 1.2$ the flow is quasi-periodic-I (characterized by the presence of a secondary frequency) and its wake is structured (figure 33*b*). At this spacing, the vortices grow behind the cylinders alternately from the top and bottom sides, and are periodically affected by the downstream cylinder before shedding; the spacing is not large enough to allow the vortex to grow completely and then shed (figure 7). This interference does not allow the pressure to build up or reduce to a level which would have caused the lift signal to be synchronous. Instead, the maximum lift developed on the cylinder in due course either reduces or increases depending on the side (top or bottom) at which the vortex is growing. This phenomenon occurs periodically and leads to the development of a secondary frequency in the signal of the lift coefficient. The pressure contours behind the cylinders indicate variation with a period which indeed corresponds to its secondary time period (not shown), thereby confirming this proposition. (Note that in figure 8 the variation in pressure corresponds to a primary cycle, whereas modulation in the pressure time series corresponds to a secondary cycle.)

At larger spacing, the vortex is shed in the gap between the cylinders. The downstream cylinder interferes with the wake, which again leads to a secondary frequency. However, now the vortex is almost on the verge of shedding and the pressure variations are relatively more severe. This leads to dominance of the

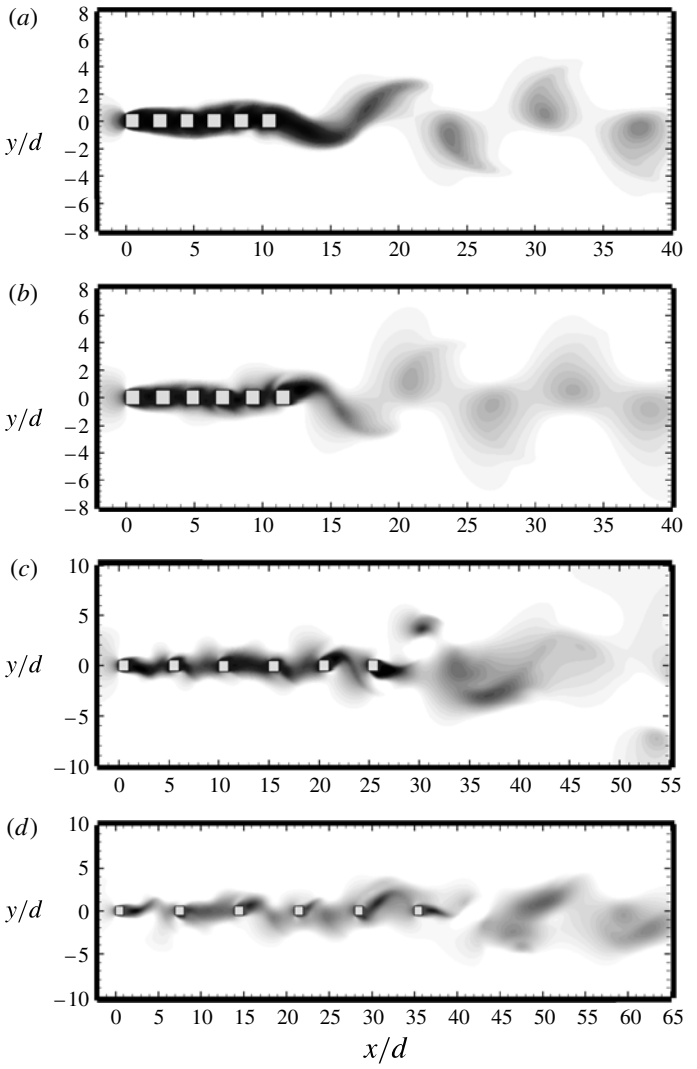

FIGURE 33. Instantaneous wakes for (*a*) $s/d = 1.0$, (*b*) $s/d = 1.2$, (*c*) $s/d = 4.0$ and (*d*) $s/d = 6.0$ at $Re = 100$. Note that the wake is the region in which the streamwise velocity is less than the free-stream velocity (Zdravkovich 1997).

secondary frequency over the primary frequency. The nature of the wake does not remain structured, owing to the increased lateral movement of the fluid in and out of the gap (figures 11 and 15). This lateral movement increases with an increase in the spacing, leading to either a quasi-periodic-II or chaotic regime. The transition of flow regimes should indeed cause the nature of forces on the cylinders to change, as already noted in the earlier sections.

The negative mean drag coefficient acting on the downstream cylinder in the case of two in-line cylinders is reported by many researchers. In the present study, at small spacing ($s/d < 2.0$ and $Re = 100$), as the flow occurs over the first cylinder the pressure behind the first cylinder does not reduce to the level it would have been in the single-cylinder case. For a single cylinder, the pressure is lowest at the back surface

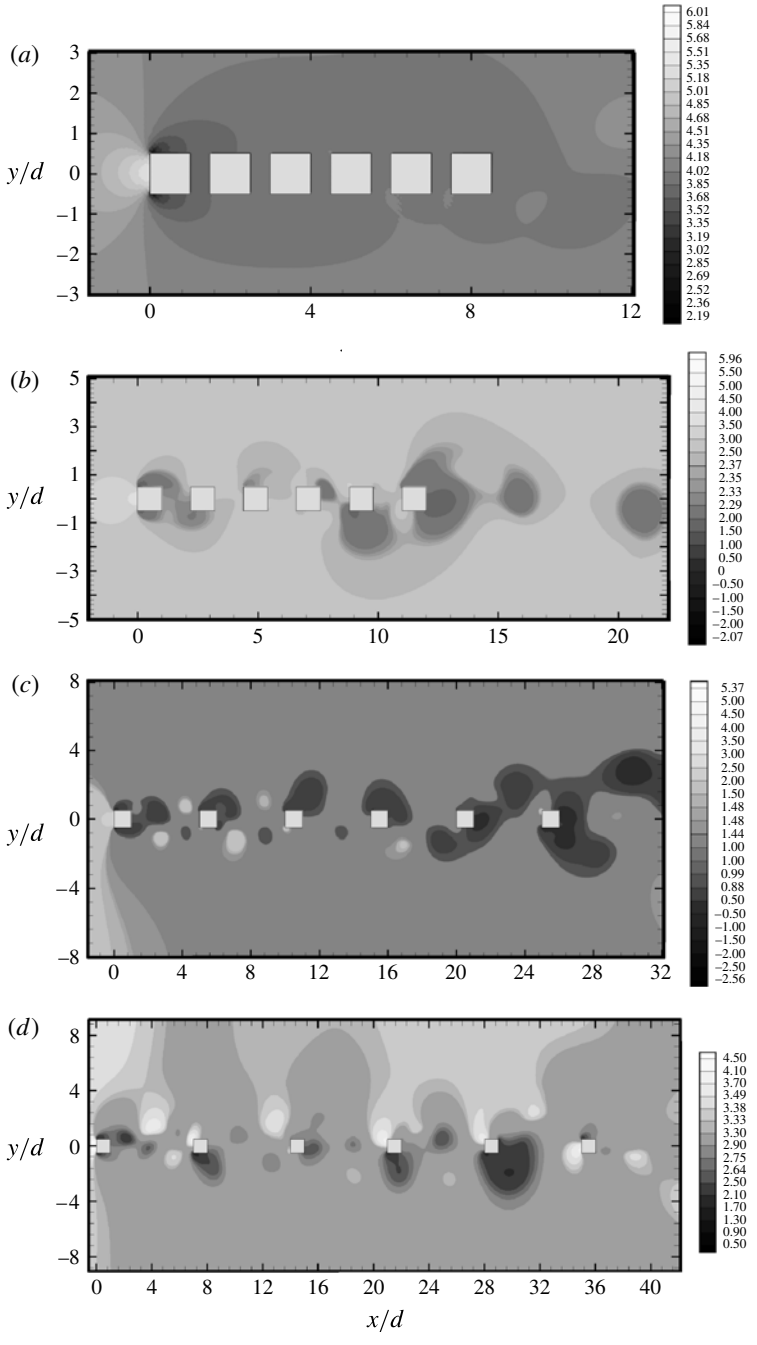

FIGURE 34. Instantaneous pressure contours for (*a*) $s/d = 0.5$, (*b*) $s/d = 1.2$, (*c*) $s/d = 4.0$ and (*d*) $s/d = 6.0$ at $Re = 100$.

of the cylinder. Figure 34 indicates that the pressure between the first and second cylinders is comparatively higher. If the shear layer from the first cylinder goes into the gap between the second and third cylinders (as in figure 11*a*), the pressure in this

gap is comparatively large and therefore the second cylinder experiences negative drag. The streamlines shown in figures 3(*b*,*e*), 7(*b*) and 11(*b*,*e*) indicate the flow of the fluid from bottom (top) to top (bottom). If the spacing is smaller the fluid is forced with higher pressure between the cylinders compared with the case of larger spacing. This causes the drag on the second cylinder to be more negative at smaller spacing. The value of negative drag reduces with successive downstream cylinders and increase in spacing, and becomes positive at larger spacing (figure 31).

The instantaneous lift force on all the cylinders (except the first) at spacings between 2.0–3.5 is larger than the instantaneous drag force experienced by these cylinders (figures 31 and 32). This is an important observation, which does not seem to have been reported before. A related observation is that the frequency of unsteady flow (represented by Strouhal number in figure 30) for all the cylinders in the case of in-line cylinders is less than for a single cylinder, whereas the amplitude of unsteady flow (represented by C_{Lrms} in figure 32) for all the cylinders is larger than for a single cylinder (except for the first cylinder). This may be due to the strong time-varying lateral forces in the in-line configuration noted above.

The mean drag and r.m.s. lift coefficients show peculiar variation in the range of $s/d = 2.0$–4.0 for the third to sixth cylinders in that they exhibit a sudden drop in this range (figures 31 and 32). The mean drag and r.m.s. lift coefficients on the second cylinder continue to increase with spacing as the vortices grow in strength in the gap and vortices shed by the first cylinder hit the second cylinder on the front face (figure 11*d*). However, for the third cylinder, because the vortex which is shed by the second cylinder reaches the rear surface of the third cylinder (figure 11*d*), these parameters show a sudden drop beyond $s/d = 3.5$. With a further increase in spacing ($s/d \geqslant 5.0$), the vortex shed by the second cylinder again hits the third cylinder at its front surface leading to an increase in the mean drag and r.m.s. lift coefficients. Similar observations apply to the fourth, fifth and sixth cylinders. This phenomenon of wake interference is consistent with that of drag inversion range and possible states reported by Carmo, Meneghini & Sherwin (2010*b*) for two circular cylinders.

It is therefore observed that wake interference is the phenomenon which governs the type of flow regime and the flow parameters experienced by in-line cylinders.

9. Concluding remarks

Numerical and *experimental* results for flow across six in-line square cylinders are presented in this paper. The flow regimes and the variation of flow parameters such as Strouhal number, mean drag and r.m.s. lift coefficients with spacing and Reynolds number have been obtained. Four basic flow regimes are initially proposed as a function of spacing for $Re = 100$; these are *synchronous* ($s/d \leqslant 1.1$), *quasi-periodic-I* ($1.2 \leqslant s/d \leqslant 1.3$), *quasi-periodic-II* ($1.4 \leqslant s/d \leqslant 5.0$), and *chaotic* ($s/d \geqslant 6.0$). These regimes are defined by studying the power spectra and the contribution of the secondary frequency to the lift coefficient signal. The existence of these *basic* flow regimes have been further checked to understand the effect of Reynolds number. The formation of a single wake behind all the cylinders (single body behaviour) makes the flow synchronous, while growth and shedding in the gap region leads the flow to move to the quasi-periodic-I, quasi-periodic-II or chaotic regimes. Whereas the synchronous regime can be characterized by a single frequency, two distinct frequencies are present in the other regimes. The numerical results are subsequently confirmed by using the experimental data at $Re = 100$; good agreement between the two is observed. For comparison, the flow for a row of square cylinders is synchronous for large spacings and becomes progressively chaotic with a reduction in spacing. The four basic flow regimes are therefore present both for in-line cylinders (here) and for a

row of cylinders (Kumar *et al.* 2008), but with a change in order with respect to the spacing and Reynolds number. The different flow regimes are further confirmed through vorticity contours for row and in-line configurations. It would be interesting to verify that the same regimes exist for other configurations of cylinders, irrespective of their number, location and geometrical parameters.

The Strouhal number corresponding to vortex shedding experienced by the cylinders is the same for all the cylinders, especially in the synchronous and quasi-periodic-I flow regime. The Strouhal number reaches a minimum at $s/d = 1.0$ for all Reynolds numbers; it increases rapidly between $1.0 < s/d < 4.0$ and slowly beyond it. Although the value of Strouhal number for a single cylinder is not recovered at the highest spacing investigated here ($s/d = 10$), it is expected to be achieved for a very large spacing free of wake interference effects. The mean drag experienced by all the cylinders (and therefore the average drag per cylinder) for an in-line arrangement is less than the mean drag on an isolated cylinder, irrespective of the spacing and Reynolds number. The drag on the first cylinder is almost constant; however, it is negative for the second cylinder. The value of negative drag reduces with an increase in the spacing and becomes positive for $s/d > 2.0$. The third cylinder also experiences negative drag at small spacings. The fourth cylinder is drag-free at $s/d = 0.5$; the drag on the fifth and sixth cylinders is always positive. The r.m.s. lift for the first three cylinders increases with spacing, reaches a maximum at around $s/d = 3$ to 4 and decreases further with increase in the spacing. With change in the spacing, the value of C_{Lrms} of the first cylinder remains close to the value for a single cylinder ($C_{Lrms} = 0.19$), but it reaches a much larger value of $\sim$1.0 for the second and third cylinders at $s/d = 3.5$. The variation of C_{Lrms} with spacing for the fourth, fifth and sixth cylinders shows abrupt changes in values at about $s/d = 2.5$–6.0. These changes are consistent with the corresponding abrupt changes in mean drag coefficient.

It is therefore noticed that the scale of wake interference is influenced by the spacing between the cylinders and the Reynolds number, which also alters the nature and magnitude of the forces acting on the cylinders. The results for such a large number of square cylinders actually present in the domain are not readily available.

Acknowledgement

The financial support of the Department of Science and Technology, New Delhi, is acknowledged.

REFERENCES

AGRAWAL, A. & AGRAWAL, A. 2006 Three-dimensional simulation of gaseous slip flow in different aspect ratio microducts. *Phys. Fluids* **18**, 103604.

AGRAWAL, A., DJENIDI, L. & ANTONIA, R. A. 2006 Investigation of flow around a pair of side-by-side square cylinders using the lattice Boltzmann method. *Comput. Fluids* **35**, 1093–1107.

CARMO, B. S., MENEGHINI, J. R. & SHERWIN, S. J. 2010*a* Secondary instability in the flow around two circular cylinders in tandem. *J. Fluid Mech.* **644**, 395–431.

CARMO, B. S., MENEGHINI, J. R. & SHERWIN, S. J. 2010*b* Possible states in the flow around two circular cylinders in tandem with separations in the vicinity of the drag inversion spacing. *Phys. Fluids* **22**, 054101.

CHEN, S. & DOOLEN, G. D. 1998 Lattice Boltzmann method for fluid flows. *Annu. Rev. Fluid Mech.* **30**, 329–364.

DJENIDI, L. 2006 Lattice-Boltzmann simulation of grid-generated turbulence. *J. Fluid Mech.* **552**, 13–35.

FRISCH, U., HASSLACHER, B. & POMEAU, Y. 1986 Lattice-gas automata for the Navier–Stokes equations. *Phys. Rev. Lett.* **56**, 1505–1508.

HARICHANDAN, A. B. & ROY, A. 2010 Numerical investigation of low Reynolds number flow past two and three circular cylinders using unstructured grid CFR scheme. *Intl J. Heat Fluid Flow* **31**, 154–171.

HETZ, A. A., DHAUBHADEL, M. N. & TELIONIS, D. P. 1991 Vortex shedding over five in-line cylinders. *J. Fluids Struct.* **5**, 243–257.

KIM, M. K., KIM, D. K., YOON, S. H. & LEE, D. H. 2008 Measurements of the flow fields around two square cylinders in tandem arrangement. *J. Mech. Sci. Technol.* **22**, 397–407.

KUMAR, S. R., SHARMA, A. & AGRAWAL, A. 2008 Simulation of flow around a row of square cylinders. *J. Fluid Mech.* **606**, 369–397.

LANKADASU, A. & VENGADESAN, S. 2007 Interference effect of two equal-sized square cylinders in tandem arrangement: with planar shear flow. *Intl J. Numer. Meth. Fluids* **57**, 1005–1021.

LIANG, C., PAPADAKIS, G. & LUO, X. 2009 Effect of tube spacing on the vortex shedding characteristics of laminar flow past an inline tube array: a numerical study. *Comput. Fluids* **38**, 950–964.

LIU, C. H. & CHEN, J. M. 2002 Observations of hysteresis in flow around two square cylinders in a tandem arrangement. *J. Wind Engng Ind. Aerodyn.* **90**, 1019–1050.

LUO, S. C. & TENG, T. C. 1990 Aerodynamic forces on a square section cylinder that is downstream to an identical cylinder. *Aeronaut. J.* **94**, 203–212.

MENEGHINI, J. R., SALTARA, F., SIQUEIRA, C. L. R. & FERRARI, J. A. JR 2001 Numerical simulation of flow interference between two circular cylinders in tandem and side-by-side arrangements. *J. Fluids Struct.* **15**, 327–350.

MITTAL, S., KUMAR, V. & RAGHUVANSHI, A. 1997 Unsteady incompressible flows past two cylinders in tandem and staggered arrangements. *Intl J. Numer. Meth. Fluids* **25**, 1315–1344.

MIZUSHIMA, J. & SUEHIRO, N. 2005 Instability and transition of flow past two tandem circular cylinders. *Phys. Fluids* **17**, 104107.

SAHA, A. K., BISWAS, G. & MURALIDHAR, K. 2003 Three-dimensional study of flow past a square cylinder at low Reynolds numbers. *Intl J. Heat Fluid Flow* **24**, 54–66.

SAKEMOTO, H, HANIU, H. & OBATA, Y. 1987 Fluctuating forces acting on two square prisms in a tandem arrangement. *J. Wind Engng Ind. Aerodyn.* **26**, 85–103.

SEWATKAR, C. M., SHARMA, A. & AGRAWAL, A. 2009 On the effect of Reynolds number for flow around row of square cylinders. *Phys. Fluids* **21**, 083602.

SEWATKAR, C. M., SHARMA, A. & AGRAWAL, A. 2010 A first attempt to numerically compute forces on birds in V formation. *Artif. Life* **16**, 245–258.

SEWATKAR, C. M., SHARMA, A. & AGRAWAL, A. 2011 Simulation of flow across a row of transversely oscillating square cylinders. *J. Fluid Mech.* **680**, 361–397.

SEWATKAR, C. M., SHARMA, A. & AGRAWAL, A. 2012 On energy transfer in flow around a row of transversely oscillating square cylinders at low Reynolds number. *J. Fluids Struct.* **31**, 1–17.

SHARMA, A. & ESWARAN, V. 2004 Heat and fluid flow across a square cylinder in the two-dimensional laminar flow regime. *Numer. Heat Transfer* A **45**, 247–269.

SOHANKAR, A. & ETMINAN, A. 2009 Forced convection heat transfer from tandem square cylinders in cross flow at low Reynolds numbers. *Intl J. Numer. Meth. Fluids* **60**, 733–751.

SUCCI, S. 2001 *The Lattice Boltzmann Equation for Fluid Dynamics and Beyond*. Clarendon.

SUMNER, D. 2010 Two circular cylinders in cross-flow: a review. *J. Fluids Struct.* **26**, 849–899.

WANG, S., TIAN, F., JIA, L., LU, X. & YIN, X. 2010 Secondary vortex street in the wake of two tandem circular cylinders at low Reynolds number. *Phys. Rev.* E **81**, 036305.

XU, G. & ZHOU, Y. 2004 Strouhal numbers in the wake of two in-line cylinders. *Exp. Fluids* **37**, 248–256.

YEN, S. C., SAN, K. C. & CHUANG, T. H. 2008 Interactions of tandem square cylinders at low Reynolds numbers. *Expl Fluid Therm. Sci.* **32**, 927–938.

ZDRAVKOVICH, M. M. 1997 *Flow around Circular Cylinders: Fundamentals*. Oxford University Press.

ZDRAVKOVICH, M. M. 1987 The effects of interference between circular cylinders in cross flow. *J. Fluids Struct.* **1**, 239–261.